Department of Precision and Microsystems Engineering

A discontinuous Galerkin based enriched finite volume method

Rick van Tatenhove

Report no : 2022.041
Coach : Alejandro Aragón, Peter Wellens
Professor : Alejandro Aragón
Specialisation : Engineering Mechanics
Type of report : Master Thesis
Date : 10 August 2022

Final Report

A discontinuous Galerkin based enriched finite volume method

by

H.J. van Tatenhove

Student number: 4534395
Hand-in date: August 10, 2022
Supervisors: Dr.Ir. P.R. Wellens, TU Delft
Dr. A.M. Aragón, TU Delft

TU Delft

Contents

Abstract

In this report a new enriched finite volume method is introduced. This method will be particularly useful for fluid-structure interaction problems. In engineering many problems are in the domain of fluid-structure interaction. Examples of these are water in sea locks, blood flowing in vessels and sailing ships. Fluid problems are usually solved with the finite volume method (FVM), and structures in this fluid flow are handled by discretizing the fluid flow around this structure. The mesh therefore needs to be conforming around the structure, and remeshing is needed when the the structure is moving over time. Remeshing is a computationally expensive process, therefore in FEM a method called enriched FEM is developed, which removes the need for remeshing. Enriched FEM uses so-called enrichment functions; these enrichment functions decouple the structure from the mesh. This concept is implemented in the finite volume method to get an enriched FVM. In order to come up with this method; FVM and enriched FEM are compared to see if the concepts of enriched FEM can be implemented in FVM. The FE method that is used is the discontinuous Galerkin (DG) method, which is a method that uses components of FEM and FVM. It discretizes equations as in FEM, but the elements are connected using flux functions as in FVM. DG is used to develop a high-order FVM and to introduce enrichments in FVM. The result of this thesis is a method which can implement enrichment functions in FVM, such that remeshing is no longer needed. The method is compared with conforming FVM and enriched DG, and it uses less computational power than both methods. The method also recovers the optimal convergence rate for a non-conforming FVM discretization. The enrichment functions are decoupled from the FVM discretization, therefore the method can be added to existing FVM solvers without changing the non-enriched part. The method is tested on a problem where waves are generated in a box.

1 Introduction

In this report an enriched finite volume method is introduced. This new method will be used for problems with fluid-structure interfaces, also called fluid-structure interaction problems. This type of problems describes the interaction of a movable or deformable structure with a fluid flow. They are crucial in many fields of engineering and physics. Examples are blood flowing through vessels, ships sailing in water or bridges. Finite Volume Methods (FVMs) are the current standard for solving the fluid dynamic equations, because of their low computational cost and ease of implementation. On the other hand there is the finite element method (FEM). Both methods divide a so-called domain into finite-sized cells that have simple shapes like triangles or quadrangles. FVM is based on conservation: what goes into a cell must leave the cell such that conservation is guaranteed, therefore it is widely used for fluid problems. In FEM the equations that are solved are taken for each cell and an approximation of the solution is made by a polynomial function. This gives an approximate solution for one element, and the contributions of all elements together give the solution of the problem. In standard FVM, discontinuities like a fluid-structure interface, are usually addressed by conforming the discretization around the discontinuity. Remeshing is needed when the discontinuity changes over time, which is computationally an expensive process. In FEM discontinuities can be addressed with a special type of FEM called enriched FEM. Enriched FEM does not have the need for remeshing as it is locally enriching the FE approximation functions with so-called enrichment functions. The objective of this thesis is to implement these enrichment functions in FVM.

Much effort has been made by researchers to get better and more efficient numerical algorithms to solve fluid problems with fluid-structure interfaces. When an object is immersed in a fluid two types of FVMs are used. The first one is conforming FVM in which the mesh is fitted around the structure [1, 2, 3]. The second approach is non-conforming FVM; where an uniform grid is used with the object immersed in that grid. One of the latter methods is the cull-cell method, which uses a uniform grid over most of the domain with the cells cut into a smaller irregular cell in any cell intersected by the discontinuity. The method was developed for potential flow problems [4, 5, 6] and it is well described by Ingram *et al.* [7]. Later the same method was applied to the Euler equations in multiple dimensions and the shallow water equations [8, 9, 10, 11], low speed incompressible flows [12, 13] and flows with moving material interfaces [14, 15]. A second often used non-conforming FVM is the immersed boundary method (IBM), which was developed by Peskin in a study on blood flow through the heart [16]. Later it was used in many fluid-structure interaction problems [17, 18, 19, 20, 21, 22, 23, 24, 25, 26, 27]. The immersed boundary method deals with structures that do not occupy volume. It uses fibers in 2D and membranes in 3D, and it models the effect of those on the fluid motion. A rigid body can only be modelled as a collections of fibers, therefore the structural response of a rigid body cannot be captured well. In order to solve this issue the immersed domain method (IDM) is developed, where the structural response is modelled accurately [28, 29, 30, 31]. Another method that is well suited for conservative problems, like fluid problems is the discontinuous Galerkin (DG) method. It is a hybrid method between FVM and FEM, as it discretizes equations as in FEM and assembles elements together using flux functions as in FVM. DG is an active field of research. It has been used to solve all kinds of problems, including the Navier-Stokes equations [32, 33, 34], convection-diffusion problems [35, 36, 37], oil recovery problems

[38], stokes flow [39, 40] and the shallow water equations [41, 42, 43]. DG can be raised to higher polynomial orders by using high-order polynomials as shape functions [44, 45, 46]. Using higher-order DG shape functions in FVM is a natural choice as FVM can be considered as a subset of DG [34]. Much research has been done for both FEM and FVM, but little effort has been done to combine the two methods to get a high-order FVM. Xiu Ye came up with a method that combines the two by using linear DG shape functions in FVM to solve elliptic problems. He used piece-wise polynomial trial functions from discontinuous Galerkin to get a discontinuous finite volume (DFV) method [47]. Later he used this method to the Stokes flow problem [48, 49]. Another method that combines aspects from both FVM and FEM is the finite volume element (FVE) method; this method uses the control volume approach from FVM and the equations are discretized using finite element spaces [50, 51]. In this report the concepts of enrichment functions will be implemented in the FVM. The enriched finite element method came from work by Melenk and Babuska on partition of unity methods [52, 53]. Moes *et al.* started to use this method for crack propagation problems under the name XFEM [54]. The concepts of enriched FEM have been applied to FVM by Jamshidi and Fallah to solve dynamic crack propagation in solids using a method that they call the extended Finite Volume Method (EFVM) [55]. The second method where enriched FEM is introduced in FVM is for flow simulations for reservoir engineering applications [56].

What has never been considered is: the use of enrichment functions from enriched FEM using DG in the finite volume method. The result is an enriched FVM, where the discontinuities can be decoupled from the grid. Many fluid solvers nowadays use FVM, because of its ease of implementation and the fact that the method is conservative by construction. For fluid-structure interaction with moving structures over time, the mesh needs to be regenerated around the discontinuity to have a conforming mesh. These enrichment functions can be used without changing the standard FVM grid, so the already written fluid solvers can be kept and discontinuities can be described with the use of enrichment functions on top of the FVM. The steps that are taken to get a new enriched FVM are the following: first of all an overview is made of existing methods on how they discretize differential equations; these methods are FVM and DG. The method to introduce enrichments in FVM follows from this. Those enrichments can be higher order shape functions or discontinuous enrichment functions. The concepts are first introduced for a simple linear advection problem. Later, to add some practical relevance to this work, the method is applied to a set of equations called the shallow water equations. This is a set of equations for fluid motion where the vertical scale is much smaller than the horizontal scale. The practical problem is a box in which waves are generated using a wave generator. This wave generator is a horizontally moving wave board, which moves in a sinusoidal motion to generate waves. This wave board is a strong discontinuity in the domain as there is no water on one side of the board and the waves are generated on the other sides of the board.

2

An Enriched Finite Volume Method

The finite volume method (FVM) and discontinuous Galerkin (DG) method are used in this section to discretize the 1D linear advection. This is done to find the connection between both methods. The equation is given by

$$\frac{\partial q}{\partial t} + c\frac{\partial q}{\partial x} = 0, \tag{2.1}$$

where q is a conserved quantity like mass, momentum or energy. This quantity is moving with a positive advection velocity c. The chapter starts by discretizing this equation with FVM, afterwards with DG; the next step is to outline the connection between the methods. Followed by a higher-order finite volume method, and an enriched finite volume method. The newly found method is tested in the end for a practical example: the shallow water equations.

2.1. Comparing discretizations for the linear advection equation

The first numerical method is the finite volume method. FVM divides the domain in cells and in each cell a constant function value of q is assumed. It is therefore 1st-order accurate. FVM uses flux approximations of q on each cell boundary to connect different cells.

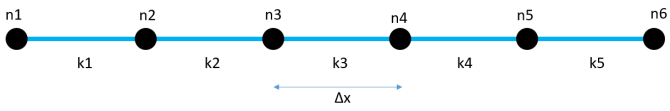

Figure 2.1: Schematic of the full 1D mesh. This mesh divides the domain in 5 cells: k1-k5. The equation is discretized for an element k, with its neighbours k-1 and k+1. The elements are connected by an upwind flux for this linear advection equation.

The equation is discretized on a finite volume cell k, as visualized in Figure 2.1. This discretization starts with the integral formulation of the equation:

$$\int_k \frac{\partial q}{\partial t} dx + \int_k c\frac{\partial q}{\partial x} dx = 0. \tag{2.2}$$

The first term of this integral formulation which is discretized is the spatial derivative, this term is also called the flux term in FVM. The values on the left and right cell boundaries are calculated using numerical fluxes, which is a mathematical concept used to calculate a quantity flowing through a surface. Different types of fluxes are possible, often central fluxes are used which take the average value of the cells at the boundary. For the linear advection equation with a positive advection velocity c, an upwind flux is used. The values on the cell faces are calculated using the value of the cell to the left of the cell face, because q is advecting from left to right. The discretized upwind scheme is given by

$$\int_k c\frac{\partial q}{\partial x} dx \approx c(q_k - q_{k-1}). \tag{2.3}$$

The second term is the time derivative. The derivative of the function value is taken to get the time derivative term. The total upwinding FVM scheme is given by

$$\frac{\partial q_k}{\partial t} = -c\frac{q_k - q_{k-1}}{\Delta x}. \tag{2.4}$$

This equation can be solved with any differential time integration scheme. For example, with the forward Euler time discretization, an RK4 scheme, or a Crank-Nicholson scheme. No integration scheme is chosen yet, so the time derivative is kept as it is. This is called a semi-discrete system, as it is discretized in space but not yet in time. The semi-discrete equation in matrix form for this 5 cell grid in Figure 2.1 is:

$$\frac{d}{dt}\begin{bmatrix} q_1 \\ q_2 \\ q_3 \\ q_4 \\ q_5 \end{bmatrix} = -\frac{c}{\Delta x}\begin{bmatrix} 1 & 0 & 0 & 0 & 0 \\ -1 & 1 & 0 & 0 & 0 \\ 0 & -1 & 1 & 0 & 0 \\ 0 & 0 & -1 & 1 & 0 \\ 0 & 0 & 0 & -1 & 1 \end{bmatrix}\begin{bmatrix} q_1 \\ q_2 \\ q_3 \\ q_4 \\ q_5 \end{bmatrix}. \tag{2.5}$$

2.2. The discontinuous Galerkin method

The same linear advection equation is now discretized with the discontinuous Galerkin (DG) method. This method uses the same discretization procedure as standard FEM, and it is very well suited for conservative problems as it uses fluxes between different elements. The method was introduced in 1973 by Reed and Hill in a study on neutron transport, and nowadays it is used in a wide variety of fluid dynamic solvers [33, 57] and solids mechanics solvers [58, 59]. It uses concepts of both FVM and FEM. DG uses piece-wise linear polynomials in its elements, but contrary to standard FEM, the polynomials are not continuous along element boundaries. This is visualized in Figure 2.2, where a standard FEM approximation is compared to a DG approximation [60].

(a) (b)

Figure 2.2: A comparison between standard FEM and DG. A part of a domain is discretized with triangular elements. (a) Standard FEM is used, which is continuous on element boundaries, (b) DG is used, which is not continuous along element boundaries.

The method is well suited for convection-diffusion problems and for capturing shocks. Contrary to FEM, it is well suited for hyperbolic problems. Problems with discontinuities or sharp gradients are another category for which DG is used. It can handle non-uniform grids with different polynomials approximations on each element. Therefore the method allows for $hp-$variants, so the grid-size and approximation order can be varied. There are a couple of advantages of DG with respect to FVM and standard FEM. DG can, contrary to FVM, easily be raised to a higher-order convergence rate. That is because in FVM piece-wise constant approximations are used, and in DG higher-order polynomials can be used. DG is also highly parallelizable, because the solution is not continuous between elements, DG can easily handle complex geometries, and the method allows for a straightforward treatment of boundary conditions [61].

The 1D linear advection equation in (2.1) is now discretized with DG. The equation is discretized on an element k; this element was visualized in Figure 2.1 in the 5-cell example. For this equation a weak form can be found by multiplying (2.1) with a weight function ϕ and integrating it over the domain Ω:

$$\int_{\Omega} \frac{\partial q}{\partial t}\phi dx + \int_{\Omega} c\frac{\partial q}{\partial x}\phi dx = 0. \tag{2.6}$$

The domain is split into K elements as in standard FEM and a local solution is defined for a particular element k. The local solutions in each element combined give the global solution of the problem. Integration by parts is used to reduce the requirement on the order of approximation functions:

$$\int_{k} \frac{\partial q}{\partial t}\phi dx + \left[cq\phi\right]_{X_L}^{X_R} - \int_{k} cq\frac{\partial \phi}{\partial x}dx = 0. \tag{2.7}$$

The elements are not connected on element boundaries as in standard FEM. As can be seen in (2.7) the DG formulation has a boundary term in it (the term in square brackets). To assemble the elements in DG, the concept of numerical flux is used. Numerical flux is also used in FVM to connect elements. Different types of flux functions can be used. With FVM upwind flux was used, so that will be used again. At the left element boundary the value of the cell to the left is used: $q(x_L) = q^{k-1}(X_R)$, and at the right element boundary the value of the cell itself: $q(x_R) = q^{k}(x_R)$. The next step is to define an approximate solution belonging to some finite vector-valued function space $\mathbf{q}^h(x,t) \in V^h$. The weight functions ϕ are as in standard FEM from the same space as the solution space: $\phi \in V^h$. For this example a linear approximation with the ramp functions is chosen. These functions are given in local coordinates for an element: $\xi \in [-1,1]$

$$\psi_1(x) = \phi_1 = \frac{1}{2}(1-\xi), \qquad \xi \in [-1,1], \tag{2.8}$$

$$\psi_2(x) = \phi_2 = \frac{1}{2}(1+\xi), \qquad \xi \in [-1,1]. \tag{2.9}$$

This gives the total approximation function for each element as:

$$q^h(\xi,t) = \sum_{i=1}^{2} \psi_i(\xi)U_i(t) = \frac{1}{2}(1-\xi)U_1(t) + \frac{1}{2}(1+\xi)U_2(t). \tag{2.10}$$

This approximation function is substituted in the weak form. The weak form must be satisfied for each weight function in an element k. So it gives j equations, where $j = 1, 2$ for the 2 linear ramp functions:

$$\int_{X_L}^{X_R} \frac{\partial q^h}{\partial t}\phi_j dx - \int_{X_L}^{X_R} cq^h\frac{\partial \phi_j}{\partial x}dx + \left[cq^h\phi_j\right]_{X_L}^{X_R} = 0 \quad \forall j \leq 2. \tag{2.11}$$

The first term in (2.11), with the time derivative, is called the mass term. The integrals in this term are solved exactly because the approximation function and the weight functions are known analytical functions. This yields a $2x2$ matrix because the weak form is valid for any weight function and the number of weight functions is 2. When higher-order shape functions are used, often the integral is not calculated exactly and a numerical quadrature rule is used to approximate it. But for the linear ramp functions, it is calculated analytically:

$$\begin{aligned}\int_{X_L}^{X_R} \frac{\partial q^h}{\partial t}\phi_j dx &= \frac{\Delta x}{2}\sum_{i=0}^{1}\frac{dU_i(t)}{dt}\int_{-1}^{1}\psi_i(\xi)\phi_j(\xi)d\xi \\ &= \frac{\Delta x}{2}\int_{-1}^{1}\begin{bmatrix}\psi_1\phi_1 & \psi_2\phi_1\\ \psi_1\phi_2 & \psi_2\phi_2\end{bmatrix}d\xi\begin{bmatrix}\frac{dU_1}{dt}\\ \frac{dU_2}{dt}\end{bmatrix} = \frac{\Delta x}{2}\begin{bmatrix}2/3 & 1/3\\ 1/3 & 2/3\end{bmatrix}\begin{bmatrix}\frac{dU_1}{dt}\\ \frac{dU_2}{dt}\end{bmatrix} = \frac{\Delta x}{2}\mathbf{M}\frac{d\mathbf{U}}{dt}.\end{aligned} \tag{2.12}$$

The second term in (2.11) is called the convection term. The convection term is derived in a similar way to the mass term, but this one involves the spatial derivatives of the weight functions:

$$\begin{aligned}\int_{X_L}^{X_R} cq^h \frac{\partial \phi_j}{\partial x} dx &= \sum_{i=0}^{1} cU_i(t) \int_{-1}^{1} \psi_i(\xi) \frac{\partial \phi_j(\xi)}{\partial \xi} d\xi \\ &= c \int_{-1}^{1} \begin{bmatrix} \psi_1\phi_1' & \psi_2\phi_1' \\ \psi_1\phi_2' & \psi_2\phi_2' \end{bmatrix} d\xi \begin{bmatrix} U_1 \\ U_2 \end{bmatrix} = c \begin{bmatrix} -1/2 & -1/2 \\ 1/2 & 1/2 \end{bmatrix} \begin{bmatrix} U_1 \\ U_2 \end{bmatrix} = c\mathbf{KU}.\end{aligned} \tag{2.13}$$

The last term in (2.11) that needs to be discretized is the flux term. As explained before this term is used to assemble the elements. Therefore it contains the subscripts k and $k-1$ for the element itself and its neighbouring element, as visualized in Figure 2.1. The derivation of this term uses the fact that both linear shape functions have value 1 at one edge and value 0 at the other edge,

$$\begin{aligned}\left[cq^h\phi_j\right]_{X_L}^{X_R} &= cq^h(X_R)\phi_j(X_R) - cq^h(X_L)\phi_j(X_L) = c \begin{bmatrix} q^h(X_R)\phi_1(X_R) - q^h(X_L)\phi_1(X_L) \\ q^h(X_R)\phi_2(X_R) - q^h(X_L)\phi_2(X_L) \end{bmatrix} \\ &= c \begin{bmatrix} -q^{k-1}(X_L) \\ q^k(X_R) \end{bmatrix} = c \begin{bmatrix} -1 & 0 & 0 \\ 0 & 0 & 1 \end{bmatrix} \begin{bmatrix} U_2^{k-1} \\ U_1^k \\ U_2^k \end{bmatrix} = c\mathbf{FU}.\end{aligned} \tag{2.14}$$

Combining the mass, convection and flux terms gives the semi-discrete system, which can be written in matrix form as:

$$\frac{\Delta x}{2}\mathbf{M}\frac{d\mathbf{U}}{dt} + c\mathbf{FU} - c\mathbf{KU} = \mathbf{0}, \tag{2.15}$$

$$\frac{\Delta x}{2} \begin{bmatrix} 2/3 & 1/3 \\ 1/3 & 2/3 \end{bmatrix} \begin{bmatrix} \frac{dU_1}{dt} \\ \frac{dU_2}{dt} \end{bmatrix} + c \begin{bmatrix} -1 & 0 & 0 \\ 0 & 0 & 1 \end{bmatrix} \begin{bmatrix} U_2^{k-1} \\ U_1^k \\ U_2^k \end{bmatrix} - c \begin{bmatrix} -1/2 & -1/2 \\ 1/2 & 1/2 \end{bmatrix} \begin{bmatrix} U_1 \\ U_2 \end{bmatrix} = \begin{bmatrix} 0 \\ 0 \end{bmatrix}. \tag{2.16}$$

The next step is to get a semi-discrete system which can be integrated in time. The matrix equation given in (2.15) can be rewritten as

$$\begin{aligned}\begin{bmatrix} \frac{dU_1}{dt} \\ \frac{dU_2}{dt} \end{bmatrix} &= \frac{2c}{\Delta x}\underline{M}^{-1}[\mathbf{K} - \mathbf{F}]\mathbf{U} = \frac{2c}{\Delta x} \begin{bmatrix} 2/3 & 1/3 \\ 1/3 & 2/3 \end{bmatrix}^{-1} \begin{bmatrix} 1 & -1/2 & -1/2 \\ 0 & 1/2 & -1/2 \end{bmatrix} \begin{bmatrix} U_2^{k-1} \\ U_1^k \\ U_2^k \end{bmatrix} \\ &= \frac{2c}{\Delta x} \begin{bmatrix} 2 & -3/2 & -1/2 \\ -1 & 3/2 & -1/2 \end{bmatrix} \begin{bmatrix} U_1^{k-1} \\ U_0^k \\ U_1^k \end{bmatrix}.\end{aligned} \tag{2.17}$$

The 5 stencil that was used for the FVM discretization in Figure 2.1 is now used for the DG discretization. This gives a sparse stencil with 10 DOFs. 2 DOFs for each element; these DOFs represent the nodal values of each element:

$$\frac{d}{dt} \begin{bmatrix} U_0^{k1} \\ U_1^{k1} \\ U_0^{k2} \\ U_1^{k2} \\ U_0^{k3} \\ U_1^{k3} \\ U_0^{k4} \\ U_1^{k4} \\ U_0^{k5} \\ U_1^{k5} \end{bmatrix} = \frac{2c}{\Delta x} \begin{bmatrix} -3/2 & -1/2 & 0 & 0 & 0 & 0 & 0 & 0 & 0 & 0 \\ 3/2 & -1/2 & 0 & 0 & 0 & 0 & 0 & 0 & 0 & 0 \\ 0 & 2 & -3/2 & -1/2 & 0 & 0 & 0 & 0 & 0 & 0 \\ 0 & -1 & 3/2 & -1/2 & 0 & 0 & 0 & 0 & 0 & 0 \\ 0 & 0 & 0 & 2 & -3/2 & -1/2 & 02 & 0 & 0 & 0 \\ 0 & 0 & 0 & -1 & 3/2 & -1/2 & 0 & 0 & 0 & 0 \\ 0 & 0 & 0 & 0 & 0 & 2 & -3/2 & -1/2 & 0 & 0 \\ 0 & 0 & 0 & 0 & 0 & -1 & 3/2 & -1/2 & 0 & 0 \\ 0 & 0 & 0 & 0 & 0 & 0 & 0 & 2 & -3/2 & -1/2 \\ 0 & 0 & 0 & 0 & 0 & 0 & 0 & -1 & 3/2 & -1/2 \end{bmatrix} \begin{bmatrix} U_0^{k1} \\ U_1^{k1} \\ U_0^{k2} \\ U_1^{k2} \\ U_0^{k3} \\ U_1^{k3} \\ U_0^{k4} \\ U_1^{k4} \\ U_0^{k5} \\ U_1^{k5} \end{bmatrix}. \tag{2.18}$$

2.2.1. High-order DG using Legendre polynomials

The linear advection equation, which was used in the previous section as an example to illustrate piece-wise linear DG, is now used again. This time an approximation with an arbitrary polynomial order will be used. The polynomials that are used are the Legendre polynomials. This is a set of polynomials that is orthogonal on a reference domain $\xi \in [-1, 1]$. The fact that they are orthogonal has favourable properties for the numerical approximation, because high-order orthogonal approximations do not produce ill-conditioned system matrices. An ill-conditioned matrix is very sensitive for numerical errors. Next to that, it also increases computational speed as recursive relations are used to calculate the polynomials [62]. The shape functions are shown in Figure 2.3. In this figure they are shown up to 5th order, but they can be raised to higher orders than that. The linear shape functions, which were used before, are also part of these functions. The Legendre polynomials are the derivatives of the shape functions.The nonlinear shape functions have value 0 at the boundaries; this makes it straightforward to apply Dirchlet boundary conditions. The Legendre Polynomial of an arbitrary order p is given by

$$L_p(\xi) = \frac{1}{p}(2p-1)\xi L_{p-1}(\xi) + (1+p)L_{p-2}(\xi). \tag{2.19}$$

The shape functions are calculated as

$$\psi_1 = \frac{1}{2}(1-\xi), \quad \psi_2 = \frac{1}{2}(1+\xi), \quad \psi_i = \hat{\psi}_{i-1}, \quad i = 3, 4, ..., p+1, \tag{2.20}$$

where

$$\psi_i = \frac{1}{\sqrt{4i-2}}(L_i(\xi) - L_{i-2}(\xi)). \tag{2.21}$$

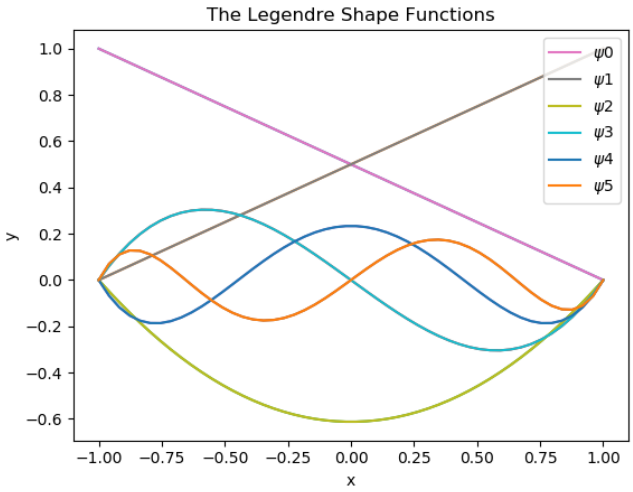

Figure 2.3: The Legendre shape functions up to 5th order. This is the set of shape functions that will be used for a high-order DG method.

The same procedure as for the linear shape functions can now be followed by deriving mass matrix, convection matrix and flux matrices. But now using the Legendre shape functions. The size of these matrices depents on the polynomial order used. The shape of the matrices is $(p+1)^2$. The derivation of the full DG scheme for the 5 cell example is left out from this report. For high-order DG it is more convenient to calculate these matrices numerically. A comparison of the 5 cell example, which discretizes a sine function as an initial condition for the linear advection equation, is given in Figure 2.4. On the left side the function is discretized with the standard linear shape functions and on the right side with cubic Legendre shape functions. As it can be seen in this figure, the cubic approximation is better with the same number of cells.

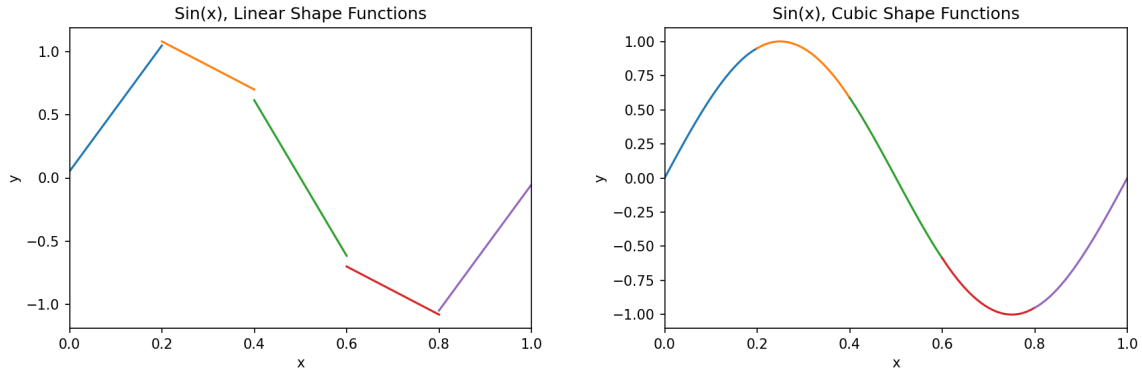

(a) (b)

Figure 2.4: A discretization of a sine function with 5 elements. It is discretized with linear shape functions (a); and cubic shape functions (b). The cubic approximation is better with the same number of cells. The use of the Legendre polynomials in DG gives therefore a more accurate approximation to the solution of the equation that is solved.

2.3. From discontinuous Galerkin to the finite volume method

DG and FVM are both numerical procedures, that are used to find a numerical approximation to the solution of a differential equation. They are therefore closely related and In this section it is proved that FEM with discontinuous elements, as in DG is the same method as FVM. The relation between the 2 methods is that the finite volume method is a piece-wise constant DG method. This holds for any equation [34], but the proof of this is given by using (2.1). The semi-discrete FVM formulation of the 1D linear advection problem was given in section 2.1 by

$$\frac{dq_k}{dt} = -c\frac{q_k - q_{k-1}}{\Delta x}. \tag{2.22}$$

For the 5-cell stencil in Figure 2.1. The discretized equation in matrix form is:

$$\frac{d}{dt}\begin{bmatrix} q_{k1} \\ q_{k2} \\ q_{k3} \\ q_{k4} \\ q_{k5} \end{bmatrix} = -\frac{c}{\Delta x}\begin{bmatrix} 1 & 0 & 0 & 0 & 0 \\ -1 & 1 & 0 & 0 & 0 \\ 0 & -1 & 1 & 0 & 0 \\ 0 & 0 & -1 & 1 & 0 \\ 0 & 0 & 0 & -1 & 1 \end{bmatrix}\begin{bmatrix} q_{k1} \\ q_{k2} \\ q_{k3} \\ q_{k4} \\ q_{k5} \end{bmatrix}. \tag{2.23}$$

The same problem is now discretized with DG, but now with constant shape functions: $\psi(x) = \phi(x) = 1$. This is similar to FVM as both methods use a constant value in each cell. The weight and approximation function are the same function as before. From the section about DG, the approximation for the linear advection problem is

$$\frac{d\mathbf{U}}{dt} = \frac{2c}{\Delta x}\mathbf{M}^{-1}[\mathbf{K} - \mathbf{F}]\mathbf{U}. \tag{2.24}$$

The mass ($\mathbf{M}$), convection ($\mathbf{K}$) and flux matrices ($\mathbf{F}$) were defined in the section about DG (section 2.2) and can be obtained using the constant shape and approximation functions. The same type of flux is used as previously for FVM and DG, namely upwind flux. There is only 1 shape function, so the matrices become scalars and they are given by

$$M = \int_{-1}^{1} \psi(\xi)\phi(\xi)dx == 2; \tag{2.25}$$

$$K = \int_{-1}^{1} \psi(\xi)\frac{\partial\phi(\xi)}{\partial\xi}d\xi = 0; \tag{2.26}$$

$$F = [\phi q^h]_{x_L}^{x_R} = \phi(x_R)q^h(x_R) - \phi(x_L)q^h(x_L) = q^k - q^{k-1} \tag{2.27}$$

The semi-discrete system for 1 cell is

$$\frac{dq_k}{dt} = \frac{2c}{\Delta x} M^{-1}[K - F] = -c\frac{q^k - q^{k-1}}{\Delta x}. \tag{2.28}$$

This can be put in a matrix form as shown below and it is thereby proved that a piece-wise constant DG discretization gives exactly the same semi-discrete scheme as FVM:

$$\frac{d}{dt}\begin{bmatrix} q_{k1} \\ q_{k2} \\ q_{k3} \\ q_{k4} \\ q_{k5} \end{bmatrix} = -\frac{c}{\Delta x}\begin{bmatrix} 1 & 0 & 0 & 0 & 0 \\ -1 & 1 & 0 & 0 & 0 \\ 0 & -1 & 1 & 0 & 0 \\ 0 & 0 & -1 & 1 & 0 \\ 0 & 0 & 0 & -1 & 1 \end{bmatrix}\begin{bmatrix} q_{k1} \\ q_{k2} \\ q_{k3} \\ q_{k4} \\ q_{k5} \end{bmatrix}. \tag{2.29}$$

2.4. A high-order finite volume method

In the previous section it was proved that FVM is actually a special type of DG. Using this, FVM can be raised to a higher polynomial order for individual cells. In this section piece-wise linear Lagrangian shape functions are used in FVM instead of the usual constant approximation in each cell. Afterwards an arbitrary polynomial order is introduced using Legendre shape functions. The standard upwind FVM scheme to discretize the linear advection was given in (2.22). Another way to look at this equation is to see it as a sum of the mass matrix, convection, and flux matrices as in (2.15). Using this the finite volume method can be raised to a higher order for an arbitrary cell. In Figure 2.5, an 1D grid is given. The green cell k_4 will be raised from a constant value to a piece-wise linear approximation, using the shape functions in (2.8) and (2.9). This gives locally an improved approximation of the solution; this can be used at locations in the domain with steep gradients. Locally remeshing would also give an improved solution at those locations, but this approach with higher-order shape functions has the advantage that nothing has to be changed to the uniform grid. The high-order functions can be added on top of the standard piece-wise constant approximations, such that the other cells still have the constant FVM approximation.

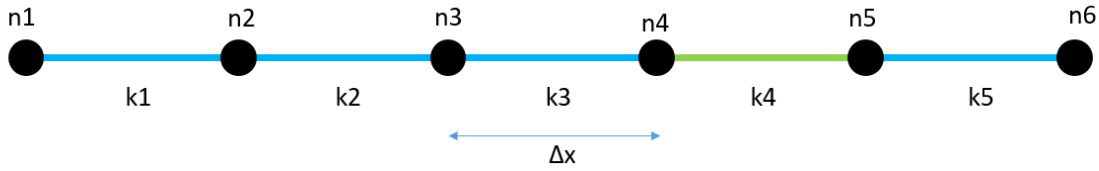

Figure 2.5: The 1D Grid with 1 high-order cell in green. All blue cells have a constant function value and cell 4 uses a high-order approximation.

As done before the mass, convection, and flux matrices are set up for this higher-order element:

$$\mathbf{M} = \int_{-1}^{1} \psi_i(\xi)\phi_j(\xi)d\xi = \int_{-1}^{1} \begin{bmatrix} \psi_1\phi_1 & \psi_2\phi_1 \\ \psi_1\phi_2 & \psi_2\phi_2 \end{bmatrix} d\xi = \begin{bmatrix} 2/3 & 1/3 \\ 1/3 & 2/3 \end{bmatrix}, \tag{2.30}$$

$$\mathbf{K} = \int_{-1}^{1} \psi_i(\xi)\frac{\partial\phi_j(\xi)}{\partial\xi}d\xi = \int_{-1}^{1} \begin{bmatrix} \psi_1\phi_1' & \psi_2\phi_1' \\ \psi_1\phi_2' & \psi_2\phi_2' \end{bmatrix} d\xi = \begin{bmatrix} -1/2 & -1/2 \\ 1/2 & 1/2 \end{bmatrix}, \tag{2.31}$$

$$\begin{aligned} \mathbf{FU} = \left[cq^h\phi_j\right]_{X_L}^{X_R} &= cq^h(X_R)\phi_j(X_R) - cq^h(X_L)\phi_j(X_L) = c\begin{bmatrix} q^h(X_R)\phi_1(X_R) - q^h(X_L)\phi_1(X_L) \\ q^h(X_R)\phi_2(X_R) - q^h(X_L)\phi_2(X_L) \end{bmatrix} \\ &= c\begin{bmatrix} -q^{k-1}(X_L) \\ q^k(X_R) \end{bmatrix} = c\begin{bmatrix} -1 & 0 & 0 \\ 0 & 0 & 1 \end{bmatrix}\begin{bmatrix} q^{k-1} \\ q_1^k \\ q_2^k \end{bmatrix}. \end{aligned} \tag{2.32}$$

After deriving all matrices, the total semi-discrete, high-order FVM scheme can be set up. This scheme can be integrated in time with any time integration scheme. In this scheme q^{k-1} is the FVM cell value at the cell $k-1$. q_0^k and q_1^k are the nodal values of the higher order cell at the left and right element edge, respectively.

$$\frac{\Delta x}{2}\mathbf{M}\frac{d\mathbf{q}}{dt} + c\mathbf{F}\mathbf{q} - c\mathbf{K}\mathbf{q} = \frac{\Delta x}{2}\begin{bmatrix}\frac{2}{3} & \frac{1}{3}\\ \frac{1}{3} & \frac{2}{3}\end{bmatrix}\begin{bmatrix}\frac{dq_0^k}{dt}\\ \frac{dq_1^k}{dt}\end{bmatrix} + c\begin{bmatrix}-1 & 0 & 0\\ 0 & 0 & 1\end{bmatrix}\begin{bmatrix}q^{k-1}\\ q_0^k\\ q_1^k\end{bmatrix} - c\begin{bmatrix}-\frac{1}{2} & -\frac{1}{2}\\ \frac{1}{2} & \frac{1}{2}\end{bmatrix}\begin{bmatrix}q_0^k\\ q_1^k\end{bmatrix} = \mathbf{0}. \quad (2.33)$$

Afterwards the system of matrix equations is solved for the time derivatives of the high-order nodal values q_0^k and q_1^k. This high-order cell can simply be inserted into the total FVM scheme. With this method there is no need to change anything to the FVM cells that are not high-order,

$$\begin{aligned}\begin{bmatrix}\frac{dq_0^k}{dt}\\ \frac{dq_1^k}{dt}\end{bmatrix} &= \frac{2c}{\Delta x}\begin{bmatrix}\frac{2}{3} & \frac{1}{3}\\ \frac{1}{3} & \frac{2}{3}\end{bmatrix}^{-1}\left(\begin{bmatrix}-\frac{1}{2} & -\frac{1}{2}\\ \frac{1}{2} & \frac{1}{2}\end{bmatrix}\begin{bmatrix}q_0^k\\ q_1^k\end{bmatrix} - \begin{bmatrix}-1 & 0 & 0\\ 0 & 0 & 1\end{bmatrix}\begin{bmatrix}q^{k-1}\\ q_0^k\\ q_1^k\end{bmatrix}\right)\\ &= \frac{2c}{\Delta x}\begin{bmatrix}2 & -1\\ -1 & 2\end{bmatrix}\begin{bmatrix}1 & -\frac{1}{2} & -\frac{1}{2}\\ 0 & \frac{1}{2} & -\frac{1}{2}\end{bmatrix}\begin{bmatrix}q^{k-1}\\ q_0^k\\ q_1^k\end{bmatrix} = \frac{c}{\Delta x}\begin{bmatrix}4 & -3 & -1\\ -2 & 3 & -1\end{bmatrix}\begin{bmatrix}q^{k-1}\\ q_0^k\\ q_1^k\end{bmatrix}.\end{aligned} \quad (2.34)$$

The total FVM scheme for the example in Figure 2.5 is now set up. The standard constant FVM approximations are used in all cells, except for one cell where the piece-wise linear approximation is used (cell k_4). This semi-discrete scheme contains the cell values of each cell, but for the high-order cell it contains the nodal values q_{n4} and q_{n5} displayed in green,

$$\frac{d}{dt}\begin{bmatrix}q_{k1}\\ q_{k2}\\ q_{k3}\\ q_{n4}\\ q_{n5}\\ q_{k5}\end{bmatrix} = -\frac{c}{\Delta x}\begin{bmatrix}1 & 0 & 0 & 0 & 0 & 0\\ -1 & 1 & 0 & 0 & 0 & 0\\ 0 & -1 & 1 & 0 & 0 & 0\\ 0 & 0 & -4 & 3 & 1 & 0\\ 0 & 0 & 2 & -3 & 1 & 0\\ 0 & 0 & 0 & 0 & -1 & 1\end{bmatrix}\begin{bmatrix}q_{k1}\\ q_{k2}\\ q_{k3}\\ q_{n4}\\ q_{n5}\\ q_{k5}\end{bmatrix}. \quad (2.35)$$

The high-order cell is also visualized in Figure 2.6. In this figure a sine function is used as an initial condition. This sine function is discretized with standard FVM in the left side figure, and in the right side figure FVM with one higher order, piece-wise linear cell is used. The approximation is more accurate at this location. This is useful for problems with a steep gradient locally.

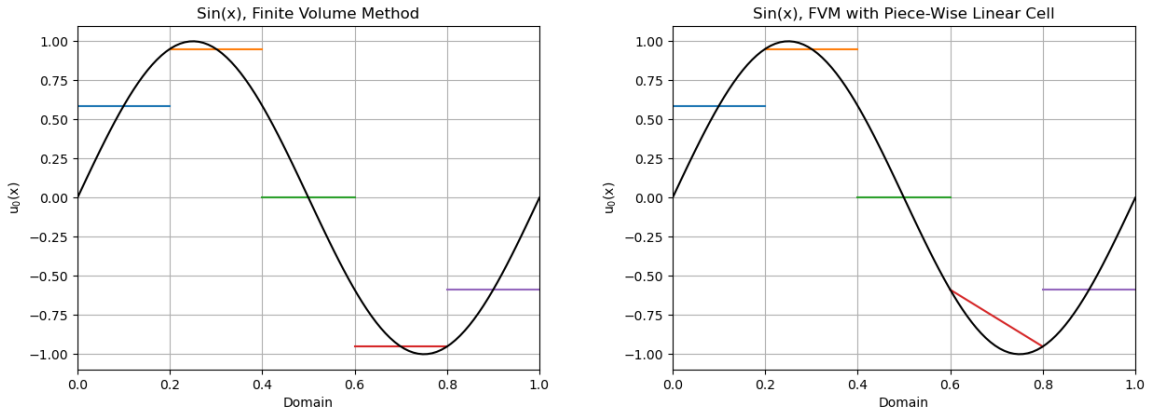

(a) (b)

Figure 2.6: A discretization of a sine function with 5 elements. The exact function is given in black. (a) Discretization with standard FVM; (b) discretization with a piece-wise linear approximation in the 4th cell. This cell gives locally an improved approximation of the solution.

2.4.1. An arbitrary high-order finite volume method

The next step is to add an arbitrary high-order polynomial approximation in the FVM scheme. The Legendre polynomials, which were introduced in subsection 2.2.1, are used again here. The linear Legendre shape functions, which were used before are also part of these functions. The same procedure as used for the linear higher-order shape functions is followed. We start by deriving the mass, convection, and flux matrices, but this time the Legendre shape functions are used. The green cell in Figure 2.5, which had a piece-wise linear approximation in the previous section, now has a piece-wise cubic approximation function. The shape functions for this cell are the first 4 Legendre polynomial shape functions which were defined in subsection 2.2.1. The higher order FVM scheme is derived numerically, and it gives the semi-discrete scheme as

$$\frac{d}{dt}\begin{bmatrix} q_{k1} \\ q_{k2} \\ q_{k3} \\ q_{n4} \\ q_{\psi_2} \\ q_{\psi_3} \\ q_{n5} \\ q_{k5} \end{bmatrix} = -\frac{c}{\Delta x}\begin{bmatrix} 1 & 0 & 0 & 0 & 0 & 0 & 0 & 0 \\ -1 & 1 & 0 & 0 & 0 & 0 & 0 & 0 \\ 0 & -1 & 1 & 0 & 0 & 0 & 0 & 0 \\ 0 & 0 & -16 & 15 & -2.45 & 3.16 & 1 & 0 \\ 0 & 0 & -12.25 & 12.25 & 0 & 7.75 & 0 & 0 \\ 0 & 0 & 22.14 & 22.14 & 0 & 0 & 0 & 0 \\ 0 & 0 & 4 & -5 & 2.45 & 3.16 & 1 & 0 \\ 0 & 0 & 0 & 0 & 0 & 0 & -1 & 1 \end{bmatrix}\begin{bmatrix} q_{k1} \\ q_{k2} \\ q_{k3} \\ q_{n4} \\ q_{\psi_2} \\ q_{\psi_3} \\ q_{n5} \\ q_{k5} \end{bmatrix} \tag{2.36}$$

In this scheme the values q_k are the cell values of the normal low order cells. The values q_{n4} and q_{n5} are the nodal values of the green 3th-order cell. And the values $q_{\psi 2}$ and $q_{\psi 3}$ are the coefficients of the quadratic and cubic shape functions used in the green cell. Those last two values do not have a physical meaning. The whole set of shape functions needs to be evaluated in order to find values at each position of the high-order, cubic FVM cell. In Figure 2.7 the high-order FVM is compared with the standard FVM for the discretization of a sine function.

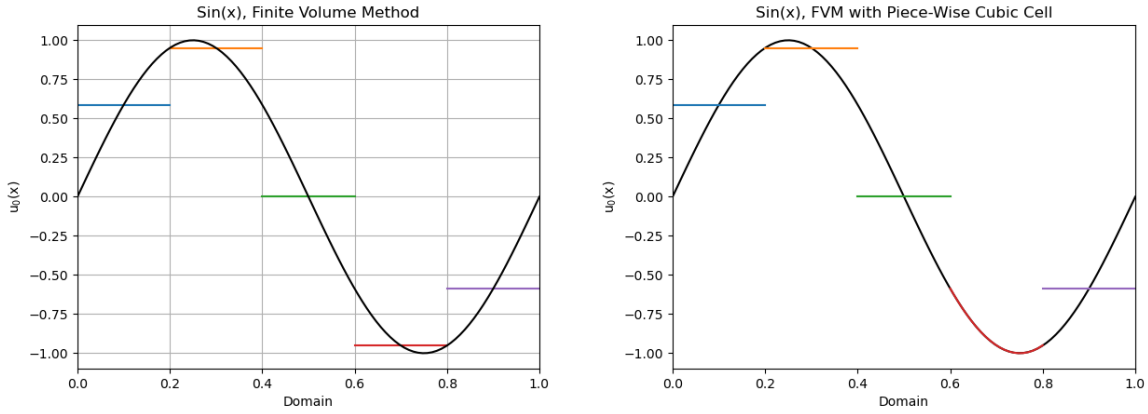

(a) (b)

Figure 2.7: A discretization of a sine function with 5 elements. The exact function is given in black. (a) Discretization with standard FVM; (b) discretization with a piece-wise cubic approximation in the 4th cell. This cubic approximation gives locally an accurate representation of the function.

2.5. The enriched discontinuous Galerkin method

In standard FEM and the conforming finite volume method, discontinuities or interfaces are usually handled by remeshing; the mesh is changed to a confirming mesh around the discontinuity. Remeshing is a computationally expensive process, but remeshing in FEM is no longer necessary with the introduction of a method called GFEM [63]. This method uses a priori knowledge about the solution of the problem to improve the standard FEM solution. The discontinuities in these problems can be completely decoupled from the mesh so remeshing is no longer needed. The type of enriched FEM that will be used, is DE-FEM [64]. This is a type of enriched FEM that has the mesh independent nature of enriched FEM, but contrary to most other enriched methods essential boundary conditions can be applied in the same way as standard FEM. This works because the functions are local by construction and have no

value at the element edges. DE-FEM can be used for problems with strong and weak discontinuities. A strong discontinuity is a jump in the solution and weak discontinuity is a jump in the gradient of the solution. For now only problems with strong discontinuities are considered, but the method can also be extended for problems with both strong and weak discontinuities. The enrichment function for strong discontinuities is visualized in Figure 2.8 on the reference domain $[-1, 1]$. The shape function with a unit jump is given as

$$\chi(\xi, t) = \begin{cases} -\frac{1}{2}(\xi + 1), & \text{if } \xi < x_{\mathrm{T}}(t), \\ -\frac{1}{2}(\xi - 1), & \text{if } \xi > x_{\mathrm{T}}(t), \end{cases} \tag{2.37}$$

where $x_{\mathrm{T}}(t)$ is the discontinuity location in local coordinates.

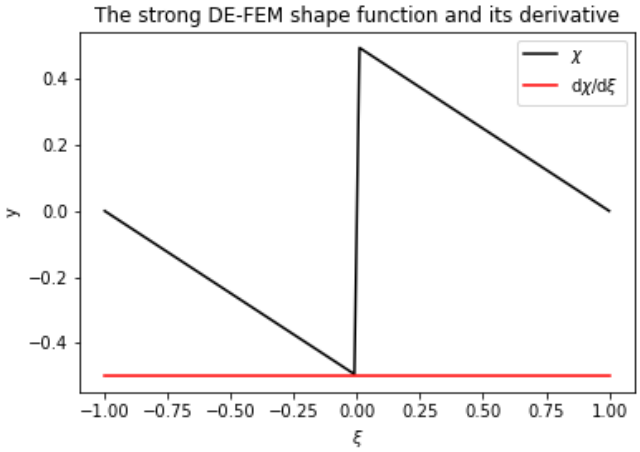

Figure 2.8: The DE-FEM shape function χ used to capture strong discontinuities, and its spatial derivative. A strong discontinuity in the solution field can be recovered with the unit jump in the shape function. In this figure the jump is at $\xi = 0$, but it can be at any position x_{T} in the enriched element.

The total approximation function for the enriched element is the sum of the standard linear shape functions, and the strong DE-FEM shape function:

$$u^h(x, t) = \sum_{i \in I_h} \psi_j(\xi) U_j(t) + \chi(\xi, t)\beta(t). \tag{2.38}$$

Having this total approximation it is now possible to set up the mass, convection and flux matrices for an enriched element. Bubnov-Galerkin FEM is used, such that the approximation functions $\psi(\xi)$ are the same as the weight functions $\phi(\xi)$. The DE-FEM shape function given in (2.37) is now used as the third shape function. This gives the following symmetric, enriched matrix:

$$\mathbf{M} = \int_{x_L}^{x_R} \psi_i(x)\phi_j(x)dx = \Delta x \int_{-1}^{1} \psi_i(\xi)\phi_j(\xi)d\xi = \Delta x \int_{-1}^{1} \begin{bmatrix} \psi_1\phi_1 & \psi_2\phi_1 & \chi\phi_1 \\ \psi_1\phi_2 & \psi_2\phi_2 & \chi\phi_2 \\ \psi_1\chi & \psi_2\chi & \chi\chi \end{bmatrix} d\xi. \tag{2.39}$$

The convection matrix is constructed using the integral over the approximation functions times the derivative of the weight functions. That gives the following enriched matrix:

$$\mathbf{K} = \int_{x_L}^{x_R} \psi_i(x) \frac{\partial \phi_j(x)}{\partial t} dx = \int_{-1}^{1} \psi_i(\xi)\phi_j'(\xi)d\xi = \int_{-1}^{1} \begin{bmatrix} \psi_1\phi_1' & \psi_2\phi_1' & \chi\phi_1' \\ \psi_1\phi_2' & \psi_2\phi_2' & \chi\phi_2' \\ \psi_1\chi' & \psi_2\chi' & \chi\chi' \end{bmatrix} d\xi. \tag{2.40}$$

The last matrix for the enriched element is the enriched flux matrix. The flux matrix contains the multiplication of the approximation functions with the weight functions. The enrichment function χ is zero on element edges. Therefore, the last row is zero. The weight functions ϕ_1 and ϕ_2 are also 0 on the

right and left edge, respectively, and they have value 1 on the other edge. Upwind flux is used for this advection problem, and therefore the enriched matrix is given by

$$\begin{aligned}\mathbf{FU} &= [u^h(x)\phi_j(x)]_{x_L}^{x^R} = [u^h(X)\phi_j(X)]_{-1}^{1} = \begin{bmatrix} u^h\phi_1 \\ u^h\phi_2 \\ u^h\chi \end{bmatrix}\Bigg|_{-1}^{1} \\ &= \begin{bmatrix} u^h(1)\phi_1(1) \\ u^h(1)\phi_2(1) \\ u^h(1)\chi(1) \end{bmatrix} - \begin{bmatrix} u^h(-1)\phi_1(-1) \\ u^h(-1)\phi_2(-1) \\ u^h(-1)\chi(-1) \end{bmatrix} = \begin{bmatrix} -1 & 0 & 0 & 0 \\ 0 & 0 & 1 & 0 \\ 0 & 0 & 0 & 0 \end{bmatrix} \begin{bmatrix} U_2^{k-1} \\ U_1^k \\ U_2^k \\ \beta \end{bmatrix}\end{aligned} \tag{2.41}$$

The enriched DG scheme can now be integrated in time using (2.17). This process is equal to the time integration of the standard DG method, so it is not treated in this section. The enriched DG method is used in the next section to develop an enriched finite volume method.

2.6. An enriched finite volume method

It was shown that the finite volume method can be raised to a higher order for individual cells. The same method to introduce high-order cells in the FVM is now used to introduce enrichments in FVM. The cells with a discontinuity are the cells that will be enriched. In these cells a piece-wise linear approximation will be used, enriched with the DE-FEM shape function. This gives the following shape functions given in local coordinates, where T(t) is the position of the discontinuity in the cell in local coordinates:

$$\begin{aligned}\psi_0(\xi) &= \phi_0(\xi) = \frac{1}{2}(1-\xi), \\ \psi_1(\xi) &= \phi_1(\xi) = \frac{1}{2}(1+\xi), \\ \psi_3(\xi,t) &= \phi_3(\xi,t) = \chi(\xi,t) = \begin{cases} -\frac{1}{2}(\xi+1), & \text{if } \xi < x_{\mathrm{T}}(t) \\ -\frac{1}{2}(\xi-1), & \text{if } \xi > x_{\mathrm{T}}(t) \end{cases}.\end{aligned} \tag{2.42}$$

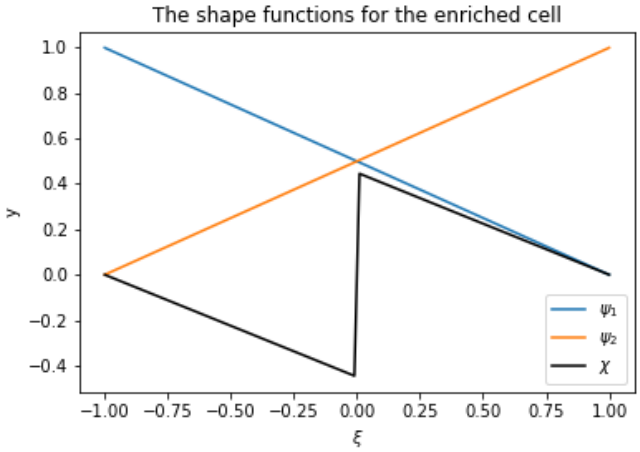

Figure 2.9: The 3 shape Functions used in the enriched cell. These 3 are the linear shape functions (ψ_1 and ψ_2), and the DE-FEM shape function (χ) to cover strong discontinuities.

The total approximation function for this enriched cell is shown in Figure 2.9. It consists of the two linear shape functions (ψ) and the DE-FEM shape function (χ):

$$u^h(\xi,t) = \sum_{i=1}^{2} \psi_i(\xi)U_i(t) + \chi(\xi,t)\beta(t) \tag{2.43}$$

The next step is to get the DE-FEM enriched finite volume scheme. This is done as before for the high-order FVM by deriving the mass, convection and flux matrices. These matrices are a function of the discontinuity position in local coordinates $x_{\mathrm{T}}(t)$. Bubnov-Galerkin FEM is used and the DE-FEM enrichment function given in (2.42) is used as the third shape function. This gives the following symmetric, enriched matrix:

$$\mathbf{M}(t) = \int_{-1}^{1} \begin{bmatrix} \psi_1\phi_1 & \psi_2\phi_1 & \chi(t)\phi_1 \\ \psi_1\phi_2 & \psi_2\phi_2 & \chi(t)\phi_2 \\ \psi_1\chi(t) & \psi_2\chi(t) & \chi(t)\chi(t) \end{bmatrix} d\xi = \begin{bmatrix} 2/3 & 1/3 & M_{13}(t) \\ 1/3 & 2/3 & M_{23}(t) \\ M_{31}(t) & M_{32}(t) & M_{33}(t) \end{bmatrix}, \tag{2.44}$$

where entries of the last row and column of the matrix are a function of the position of the discontinuity in the element:

$$\begin{aligned} M_{13}(t) &= M_{31}(t) = \frac{1}{4}x_{\mathrm{T}}^2(t) - \frac{1}{2}x_{\mathrm{T}}(t) - \frac{1}{12}, \\ M_{23}(t) &= M_{32}(t) = -\frac{1}{4}x_{\mathrm{T}}^2(t) - \frac{1}{2}x_{\mathrm{T}}(t) + \frac{1}{12}, \\ M_{33}(t) &= \frac{1}{2}x_{\mathrm{T}}^2(t) + \frac{1}{6}. \end{aligned} \tag{2.45}$$

The convection matrix is constructed using the integral over the approximation functions times the derivative of the weight functions. That gives the following enriched matrix:

$$\mathbf{K}(t) = \int_{-1}^{1} \begin{bmatrix} \psi_1\phi_1' & \psi_2\phi_1' & \chi(t)\phi_1' \\ \psi_1\phi_2' & \psi_2\phi_2' & \chi(t)\phi_2' \\ \psi_1\chi'(t) & \psi_2\chi'(t) & \chi(t)\chi'(t) \end{bmatrix} d\xi = \begin{bmatrix} -1/2 & -1/2 & K_{13}(t) \\ 1/2 & 1/2 & K_{23}(t) \\ K_{31}(t) & K_{32}(t) & K_{33}(t) \end{bmatrix}, \tag{2.46}$$

where the last row and column are again a function of the enrichment position:

$$\begin{aligned} K_{13}(t) &= K_{33}(t) = \frac{1}{2}x_{\mathrm{T}}(t), \\ K_{23}(t) &= -\frac{1}{2}x_{\mathrm{T}}(t), \\ K_{31}(t) &= K_{32} = \frac{1}{2}. \end{aligned} \tag{2.47}$$

The last term for the enriched element is the enriched flux matrix. This flux matrix is the same matrix as derived for enriched DG in (2.41). It is not a function of the discontinuity position, because a characteristic of DE-FEM is that the function values are 0 on the boundaries. The total semi-discrete, enriched scheme for the cell with the discontinuity is found with (2.17). Similar to the high-order FVM cells; this enriched cell can be added to the FVM scheme without changing anything to the existing scheme. It will add extra enriched DOFs. The physical meaning of these new DOFs is the magnitude of the jump in the solution field.

2.7. Convergence of the enriched FVM

In numerical methods it is important to analyse the numerical solution. The primary objective of the numerical solution is that it approaches the exact solution of the differential equation that is solved. This is called the convergence of the numerical solution and it consists of two main parts: consistency and stability. Consistency means that the discretization of the differential equation must be consistent with the original equation. This can be checked by substituting the Taylor series in the discretization to see if the original differential equation is found. Stability on the other hand implies whether errors grow or decay at any point during the time integration. Lax equivalence theorem states that if convergence is met. Stability and consistency are guaranteed [65]. Therefore in this section the convergence of the enriched FVM is tested with mesh refinement. The convergence properties of numerical methods over time are hard to estimate as the numerical errors are caused by both spatial and time discretizations. The goal of the enriched FVM is to add known information about the solution in the formulation. This is done by adding the DE-FEM shape functions to account for strong discontinuities in the solution. The

convergence of the method in space is tested. The discretization of a theoretical sine function is used to measure the convergence properties of this method compared to a standard FVM approximation. The initial condition that is used has a strong discontinuity in it to see how the addition of the DE-FEM helps for the convergence properties. The initial condition used is a discontinuous sine function, where $H(x)$ is the Heaviside step function and $k = 1.5$ the angular wave number:

$$f(x) = H(\frac{1}{2} - x) \cdot \sin(kx) + H(x - \frac{1}{2}) \cdot \sin(k(x-1)). \tag{2.48}$$

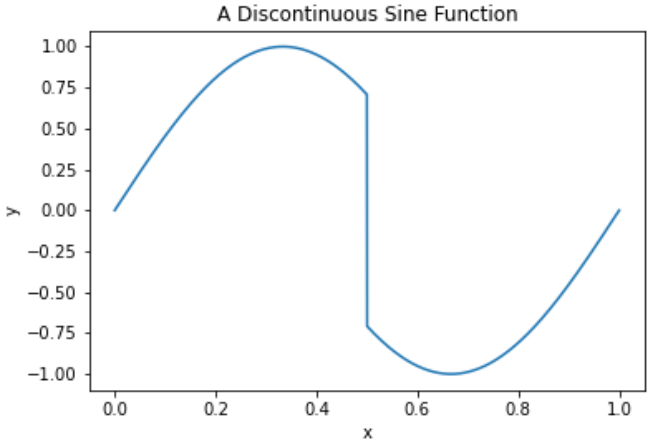

Figure 2.10: The discontinuous function that is discretized. It is a sine function with a Heaviside step function at $x = 0.5$. This function will be discretized with the standard FVM and with the new enriched FVM.

When the meshing is exactly conforming around the discontinuity the convergence rate has a value of 1, which is standard for FVM. But this optimal convergence rate is lost when the discontinuity is not exactly on the boundary between two elements. In order to regain optimal convergence, DE-FEM is used. The initial condition coefficients for the standard FVM are calculated using

$$\int_{x_L}^{x_R} \sum_{i=0}^{N} U_i \psi_i(x) \phi_j(x) dx = \int_{x_L}^{x_R} f(x) \phi_j(x) dx. \tag{2.49}$$

This a matrix equation, where the columns are the approximation functions and the rows the weight functions. For the standard, non-enriched FVM the approximation and weight functions have a value of one: ($\psi = \phi = 1$). This simplifies the equation to

$$U = \frac{\int_{x_L}^{x_R} f(x) dx}{\Delta x}. \tag{2.50}$$

In the enriched cell 3 coefficients are calculated. 2 of them are the nodal values of the cell, and 1 of them is the coefficient of DE-FEM shape function. This gives an integral matrix equation, which can be solved for the coefficients:

$$\int_{x_L}^{x_R} \begin{bmatrix} \psi_0\phi_0 & \psi_1\phi_0 & \chi(t)\phi_0 \\ \psi_0\phi_1 & \psi_1\phi_1 & \chi(t)\phi_1 \\ \psi_0\chi(t) & \psi_1\chi(t) & \chi(t)\chi(t) \end{bmatrix} dx \begin{bmatrix} U_0 \\ U_1 \\ U_2 \end{bmatrix} = \int_{x_L}^{x_R} \begin{bmatrix} f(x)\phi_0 \\ f(x)\phi_1 \\ f(x)\phi_2 \end{bmatrix} dx. \tag{2.51}$$

The exact solution is known for this manufactured function. The error with respect to the exact solution is quantified through the L^2 norm as:

$$||u - u^h||^2_{L_2(\Omega)} \tag{2.52}$$

The error is plotted for an increasing number of grid points in Figure 2.11. This is done for standard non-conforming FVM and for the enriched FVM. The enriched FVM has the optimal convergence rate of

1, which is the same as obtained with conforming FVM. For non-conforming FVM the convergence rate is almost halved to 0.55. The conclusion from this convergence study is that the DE-FEM enrichment recovers the optimal convergence for a non-conforming mesh.

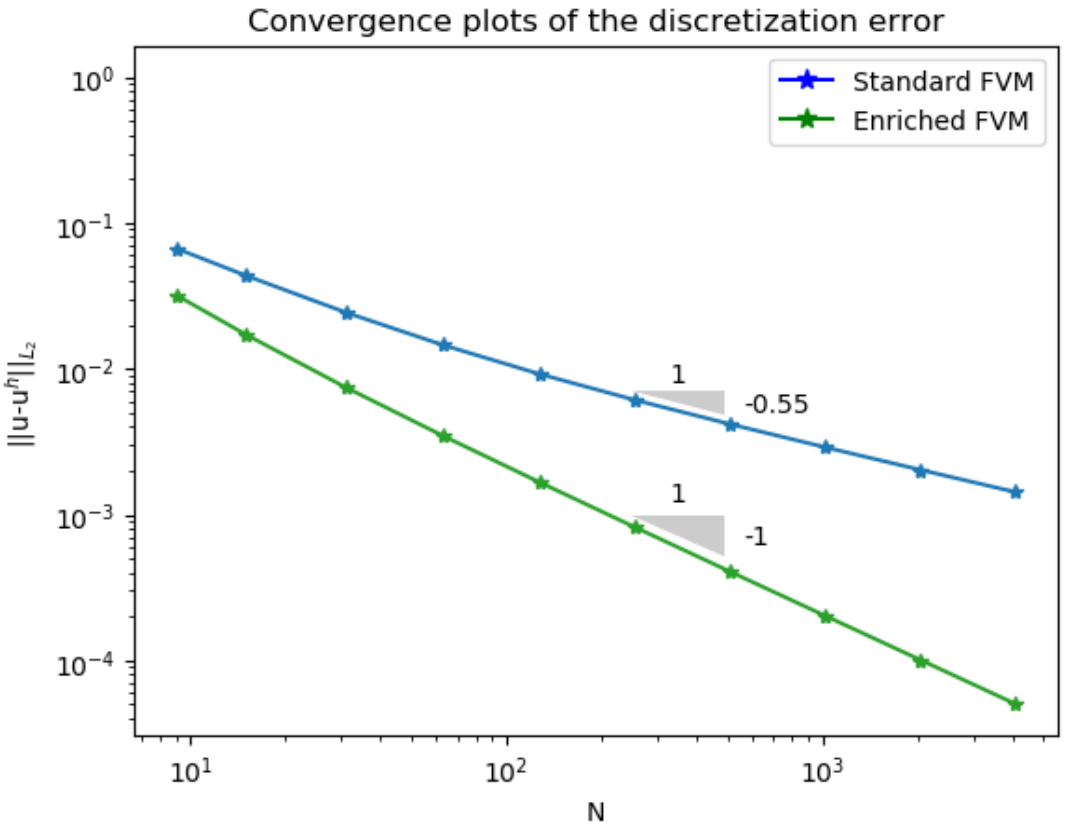

Figure 2.11: Convergence of standard, nonconforming FVM vs enriched FVM. The convergence of the method is plotted with an increasing number of elements N. The non-conforming FVM has a convergence rate of 0.55, and the enriched FVM recovers the optimal convergence rate of 1.

2.8. The shallow water equations

FVM, DG and the new enriched FVM are in this section applied to the shallow water equations, which can be used to simulate waves. The shallow water equations are a simplified subset of the Navier-Stokes equations. A schematic of this is given in Figure 2.12. The shallow water equations, from now on abbreviated as SWE, use the assumptions that the water has a constant density, and the vertical scale is much smaller than the horizontal scale. The SWE consist of 2 conservation of momentum equations, and the conservation of mass equation:

$$\begin{aligned} \frac{\partial u}{\partial t} + u\frac{\partial u}{\partial x} + v\frac{\partial u}{\partial y} + g\frac{\partial \eta}{\partial x} &= 0, \\ \frac{\partial v}{\partial t} + u\frac{\partial v}{\partial x} + v\frac{\partial v}{\partial y} + g\frac{\partial \eta}{\partial y} &= 0, \\ \frac{\partial \eta}{\partial t} + \frac{\partial hu}{\partial x} + \frac{\partial hv}{\partial y} &= 0, \end{aligned} \tag{2.53}$$

where u and v are the water velocities, g the gravitational acceleration and η the free surface of the water. The total water height is the sum of the initial water height and the free surface: $h = h_0 + \eta$.

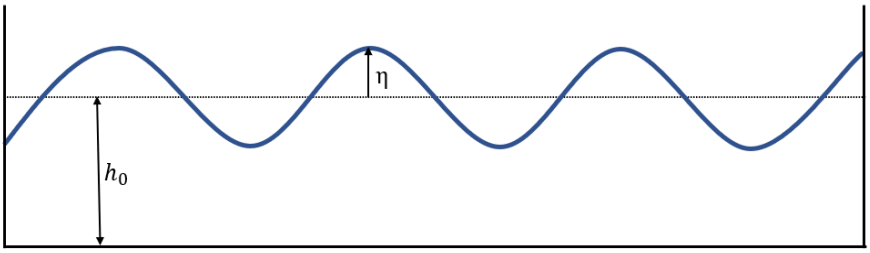

Figure 2.12: A schematic of shallow waver. On the bottom the topography of the bottom of the water is is given h, and on the top the free surface of the water η.

The given SWE can be simplified to 1 dimension by only considering the velocity in the x-direction (u). This eliminates the second momentum equation and all the terms involving v. This leaves a simplified set of 2 differential equations:

$$\frac{\partial h}{\partial t} + h_0 \frac{\partial u}{\partial x} = 0, \tag{2.54}$$

$$\frac{\partial u}{\partial t} + g \frac{\partial h}{\partial x} = 0. \tag{2.55}$$

This linearized set of equations has an analytical solution and its called the gravity wave solution. For the free surface η it is a wave oscillating in space and in time with constant amplitude A and its given by

$$\eta = A e^{ikx} e^{ikt\sqrt{gh_0}}. \tag{2.56}$$

The velocity u has exactly the same analytical solution, but scaled by the factor $\sqrt{g/h_0}$:

$$u = \sqrt{\frac{g}{h_0}} A e^{ikx} e^{ikt\sqrt{gh_0}}. \tag{2.57}$$

2.8.1. Discretization of the SWE

The linear SWE are discretized with FVM using a central difference scheme. The discretization of a differential equation with FVM was covered in detail in section 2.1. The outcomes are two semi-discrete equations, one for the water height h, and one for the water velocity u:

$$\frac{\partial h}{\partial t} = -h_0 \frac{u_{k+1} - u_{k-1}}{2\Delta x}, \tag{2.58}$$

$$\frac{\partial u}{\partial t} = -c \frac{h_{k+1} - h_{k-1}}{2\Delta x}. \tag{2.59}$$

In Figure 2.13 a 1D grid is given with 3 cells. The SWE are discretized on this example grid. The outcome is a semi-discrete system, which can be solved using a time integration scheme. In order to get a stable solution, the Crank-Nicholson implicit time integration scheme is chosen.

$$\frac{d}{dt}\begin{bmatrix} h_{k1} \\ h_{k2} \\ h_{k3} \\ u_{k1} \\ u_{k2} \\ u_{k3} \end{bmatrix} = \begin{bmatrix} 0 & 0 & 0 & 0 & -\frac{h_0}{2\Delta x} & 0 \\ 0 & 0 & 0 & \frac{h_0}{2\Delta x} & 0 & -\frac{h_0}{2\Delta x} \\ 0 & 0 & 0 & 0 & \frac{h_0}{2\Delta x} & 0 \\ 0 & -\frac{g}{2\Delta x} & 0 & 0 & 0 & 0 \\ \frac{g}{2\Delta x} & 0 & -\frac{g}{2\Delta x} & 0 & 0 & 0 \\ 0 & \frac{g}{2\Delta x} & 0 & 0 & 0 & 0 \end{bmatrix} \begin{bmatrix} h_{k1} \\ h_{k2} \\ h_{k3} \\ u_{k1} \\ u_{k2} \\ u_{k3} \end{bmatrix} \tag{2.60}$$

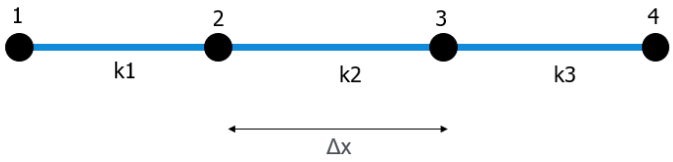

Figure 2.13: The 1D Grid that will be used to demonstrate the FVM and DG discretizations of the SWE. It consists of 3 cells, which is a very course mesh. In real simulations much more cells will be used to have an accurate representation of the waves.

2.8.2. Crank-Nicholson Time Integration

The semi-discrete system that is obtained with FVM can be solved using any time integration scheme. The most straightforward choice would be an explicit forward Euler scheme which is 1st-order accurate in time, or an explicit RK4 scheme, which is 4th order accurate in time. But those explicit schemes are not stable for a central difference scheme. Therefore, to ensure stability of the system, an implicit time integration scheme is used for (2.60). The Crank-Nicholson is a combination of the forward and backward Euler method, because it uses the average function values at time-step n and time-step $n+1$. It is an implicit method so an algebraic system of equations must be solved to get to integrate the system over time:

$$\frac{u_k^{n+1} - u_k^n}{\Delta t} = \frac{1}{2}\left[F_k^n(u, x, t, \frac{\partial u}{\partial t}, \frac{\partial^2 u}{\partial t^2}) + F_k^{n+1}(u, x, t, \frac{\partial u}{\partial t}, \frac{\partial^2 u}{\partial t^2})\right]. \tag{2.61}$$

For the system in (2.60), the Crank-Nicholson time integration is implemented in the following way. The system is a matrix equation of the form: $\dot{\mathbf{u}} = \mathbf{A}\mathbf{u}$. The terms at the known, current time step (n) go to the right hand side, and the solution vector at the new time step $(n+1)$ to the left hand side [66]. This gives a matrix equation which is solved for the solution at the next time step, where $\mathbf{I}$ is the identity matrix:

$$\mathbf{u}_k^{n+1} = \left[\mathbf{I} - \frac{1}{2}\Delta t\mathbf{A}\right]^{-1}\left[\mathbf{u}_k^n + \frac{1}{2}\Delta t\mathbf{A}\mathbf{u}_k^n\right]. \tag{2.62}$$

2.8.3. SWE with the discontinuous Galerkin method

The linear SWE are now solved with DG for an element k. The discretization of a differential equation with DG was treated in section 2.2. The system of equations is solved for the variables h and u. The approximations functions for the water height h, and water speed u are:

$$\begin{aligned} \tilde{h}(x) &= \sum_{i=1}^{2} h_i(t)\psi_i(x), \\ \tilde{u}(x) &= \sum_{i=1}^{2} u_i(t)\psi_i(x). \end{aligned} \tag{2.63}$$

In this approximation $\psi_i(x)$ are the shape functions and $h_i(t)$ and $u_i(t)$ are the coefficients for these shape functions. The physical meaning of these coefficients is the value of the numerical solution at the nodes. Using the linear shape functions gives the semi-discrete system of equations for both variables:

$$\begin{aligned} \frac{d\mathbf{h}}{dt} &= \frac{\Delta x}{2} h_0 \mathbf{M}^{-1}[\mathbf{K} - \mathbf{F}]\mathbf{u} \\ \frac{d\mathbf{u}}{dt} &= \frac{\Delta x}{2} g\mathbf{M}^{-1}[\mathbf{K} - \mathbf{F}]\mathbf{h} \end{aligned} \tag{2.64}$$

The next step is to add a discontinuity to the problem to use enrichments. The discontinuous problem, which is solved, is shown in Figure 2.14. It is a box that is filled with water. The water in this box is put into motion by the horizontal movement of a waveboard, which is positioned on the left side of the box.

The waveboard moves from the left boundary of the domain towards the right and back in a sinusoidal motion. The motion of this board generates waves and creates a discontinuity. On the left side of the waveboard the water height and water velocity are 0, and on the right side they have a finite value. This jump in magnitude is a strong discontinuity in the solution field.

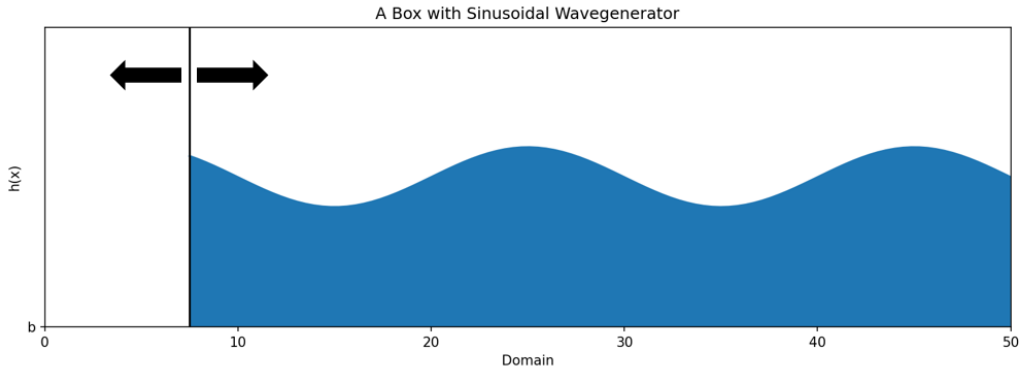

Figure 2.14: Visualization of the discontinuous problem. It is a box filled with water and waves are being generated by the sinusoidal motion of a waveboard place in the water. The waveboard creates a strong discontinuity in the solution, because the water height and velocity solutions have a jump at this position.

The problem is first solved with DG, enriched with DE-FEM. A simulation of the problem is made and shown in Figure 2.15. A wave is being generated by the movement of the waveboard, and this wave is travelling from left to right through the box. A reflecting boundary condition is set at the right wall, so when the wave hits that wall constructive interference occurs, and the amplitude of the wave increases.

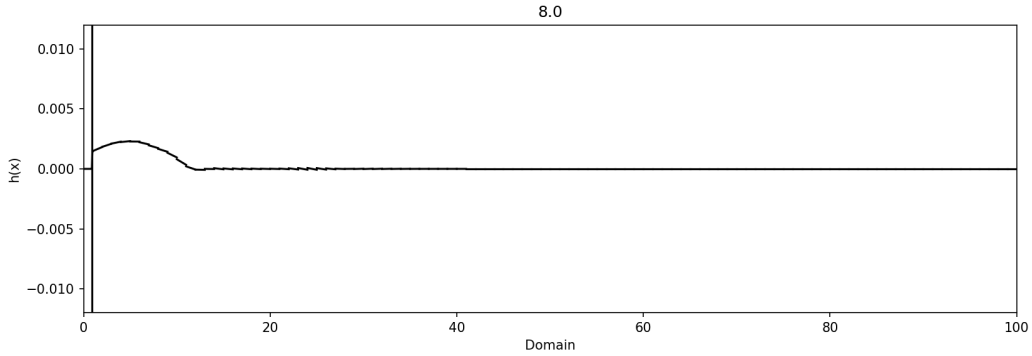

(a)

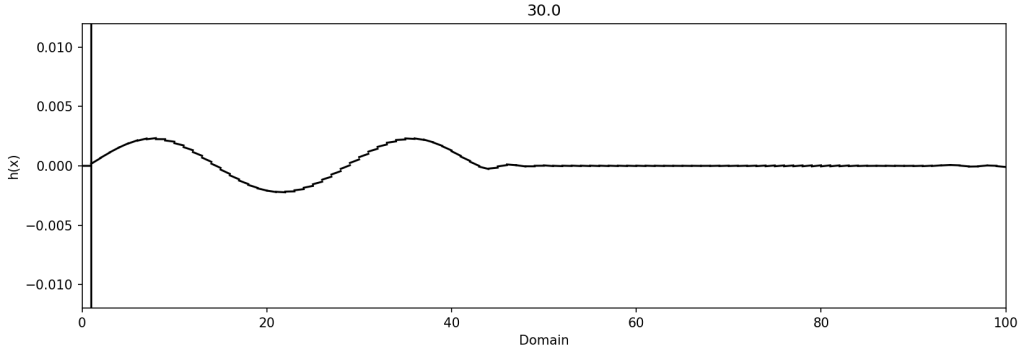

(b)

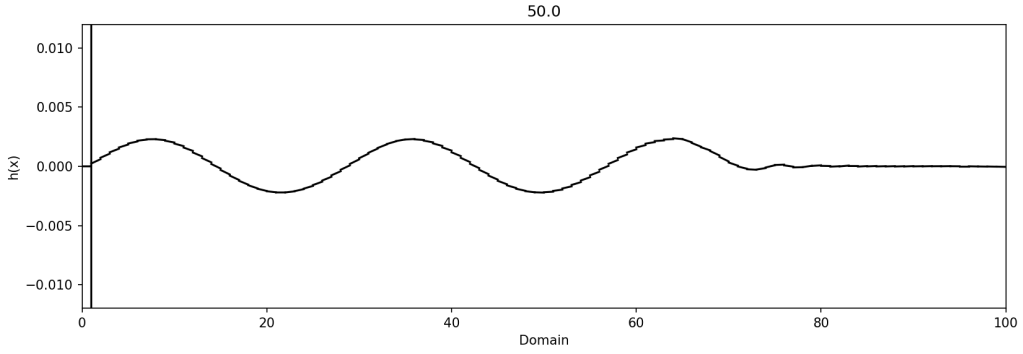

(c)

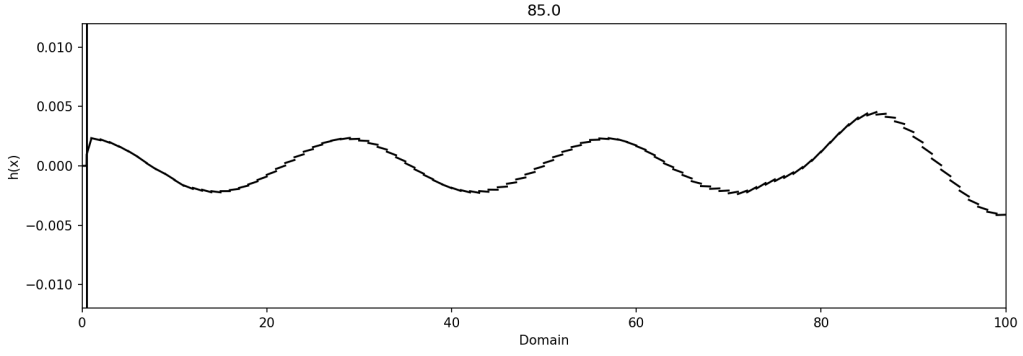

(d)

Figure 2.15: The simulation of the SWE where waves are being generated in a box. The problem is solved with an DE enriched DG method. A snapshot is taken at (a) 8s, (b) 30s, (c) 50s, and (d) 85s. The waves travel from left to right through the box, and when the right wall is hit constructive interference occurs, therefore the amplitude of the wave increases.

The enriched FVM proposed in section 2.6 is also used to solve this discontinuous problem. At the location of the waveboard, instead of a standard piece-wise constant FVM, approximation a piece-wise linear approximation with a DE-FEM enrichment will be used. The shape functions (ψ) and enrichment functions (χ) were shown in Figure 2.9. The total approximation functions for this enriched cell are given by

$$\begin{aligned} h(x,t) &= \sum_{i=1}^{2} \psi_i(x) h_i(t) + \chi(x,t)\beta_h(t), \\ u(x,t) &= \sum_{i=1}^{2} \psi_i(x) u_i(t) + \chi(x,t)\beta_u(t). \end{aligned} \tag{2.65}$$

The mass, convection and flux matrices were all derived in section 2.6. The total enriched FVM scheme for the discontinuous cell is given below for the continuity and momentum equations. This is a matrix multiplication which is solved numerically. Therefore the entries of the semi-discrete matrix are given as coefficients H_{xy} and U_{xy} instead of numerical values:

$$\begin{aligned} \frac{d}{dt}\begin{bmatrix} h_1^k \\ h_2^k \\ \beta_h \end{bmatrix} &= \frac{h_0 \Delta x}{2}\mathbf{M}^{-1}[\mathbf{K}-\mathbf{F}]\mathbf{U}_u = \begin{bmatrix} H_{11} & H_{12} & H_{13} & H_{14} \\ H_{21} & H_{22} & H_{23} & H_{24} \\ H_{31} & H_{32} & H_{33} & H_{34} \end{bmatrix}\begin{bmatrix} u^{k-1} \\ u_1^k \\ u_2^k \\ \beta_u \end{bmatrix}, \\ \frac{d}{dt}\begin{bmatrix} u_1^k \\ u_2^k \\ \beta_u \end{bmatrix} &= \frac{g \Delta x}{2}\mathbf{M}^{-1}[\mathbf{K}-\mathbf{F}]\mathbf{U}_h = \begin{bmatrix} U_{11} & U_{12} & U_{13} & U_{14} \\ U_{21} & U_{22} & U_{23} & U_{24} \\ U_{31} & U_{32} & U_{33} & U_{34} \end{bmatrix}\begin{bmatrix} h^{k-1} \\ h_0^k \\ h_1^k \\ \beta_h \end{bmatrix}. \end{aligned} \tag{2.66}$$

The enriched finite volume scheme is given for a the FVM discretization around the discontinuity. The schematic in Figure 2.13 is used with the wave board in cell k_2. The scheme is set up for these three cells of the discontinuous SWE problem. This is a part of the full enriched FVM scheme that is used to solve the problem. In cell k_1 and k_3 the standard FVM scheme is used and in cell k_2 the enriched scheme which was derived in this section,

$$\frac{d}{dt}\begin{bmatrix} h^{k1} \\ h_1^{k2} \\ h_2^{k2} \\ \beta_h \\ u^{k1} \\ u_1^{k2} \\ u_2^{k2} \\ \beta_u \end{bmatrix} = \frac{1}{2\Delta x}\begin{bmatrix} 0 & 0 & 0 & 0 & 0 & h_0 & 0 & 0 & 0 \\ 0 & 0 & 0 & 0 & H_{11} & H_{12} & H_{13} & H_{14} & H_{15} \\ 0 & 0 & 0 & 0 & H_{21} & H_{22} & H_{23} & H_{24} & H_{25} \\ 0 & 0 & 0 & 0 & H_{31} & H_{32} & H_{33} & H_{34} & H_{35} \\ 0 & g & 0 & 0 & 0 & 0 & 0 & 0 & 0 \\ U_{11} & U_{12} & U_{13} & U_{14} & 0 & 0 & 0 & 0 & 0 \\ U_{21} & U_{22} & U_{23} & U_{24} & 0 & 0 & 0 & 0 & 0 \\ U_{31} & U_{32} & U_{33} & U_{34} & 0 & 0 & 0 & 0 & 0 \end{bmatrix}\begin{bmatrix} h^{k1} \\ h_1^{k2} \\ h_2^{k2} \\ \beta_h \\ u^{k1} \\ u_1^{k2} \\ u_2^{k2} \\ \beta_u \end{bmatrix}. \tag{2.67}$$

A simulation of the enriched FVM for the wave-generaton in a box is made. The results are shown in Figure 2.16 and they give the same results as the ones obtained with enriched DG. But this time FVM is used so the approximations are continuous, which gives a smoother simulation. The waves are generated by the waveboard, and when they hit the reflecting wall on the right, the amplitude of the waves increases due to interference.

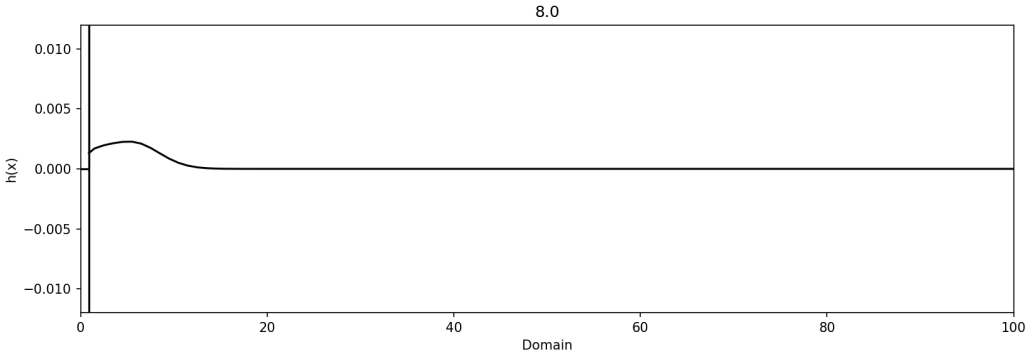

(a)

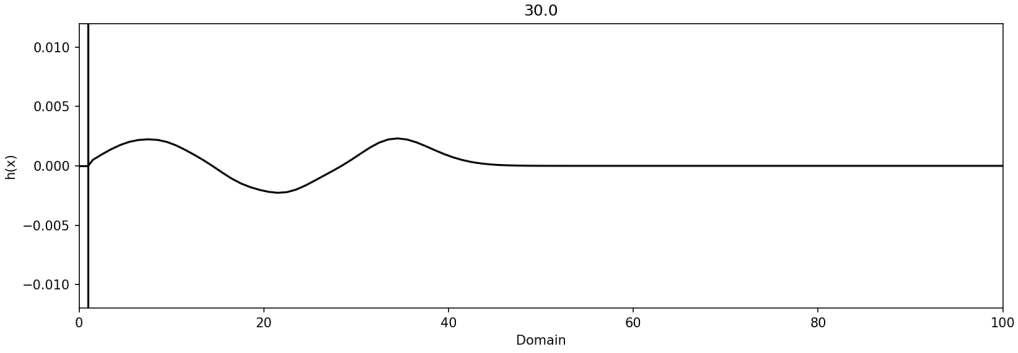

(b)

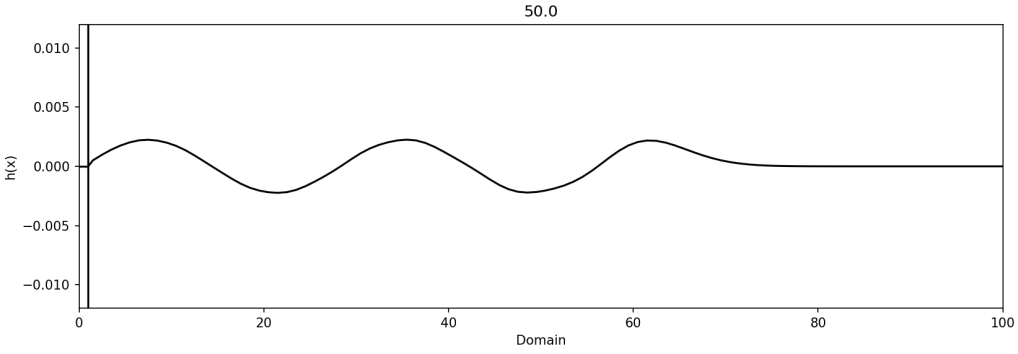

(c)

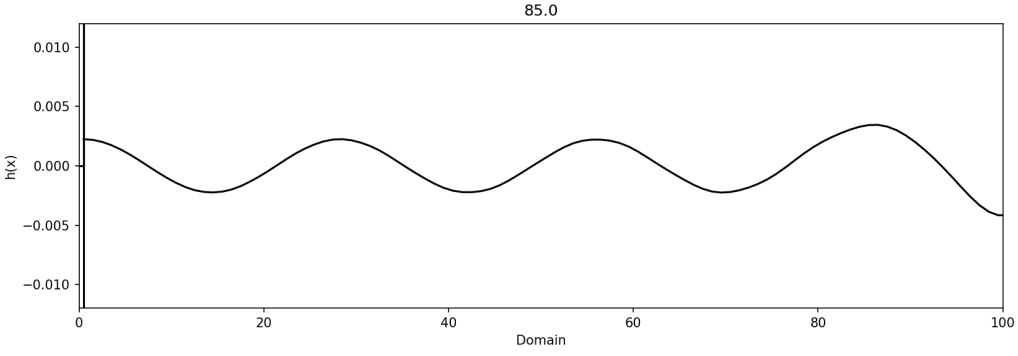

(d)

Figure 2.16: The simulation of the SWE with a sinewave as initial condition. The wave is oscillating due to gravity. A snapshot is taken at (a) 8s, (b) 30s, (c) 50s, and (d) 85s. The results of this simulation are similar to the simulation made with enriched DG, but this time it is a smooth, continuous simulation.

The goal of the enriched FVM is to save computational power by decoupling the discontinuity from the mesh, such that remeshing is no longer required due to the moving waveboard. The standard measure for the computational power, is the computational time needed to solve a problem. The conforming FVM, conforming DG, enriched DG and enriched FVM are compared for the discontinuous SWE problem. All 4 methods use the same number of elements ($N = 100$), and the same time-step ($dt = 0.01$). The results of this comparison are given in Table 2.1. The method that takes the most CPU time is the conforming DG method, as a new DG mesh needs to be generated at each time step. The enriched DG method takes less time as remeshing is no longer needed in this method. The conforming FVM is about 3 times faster than both DG methods. The reason for this is that the FVM implementation is piece-wise constant in each cell, therefore it takes less memory. The fastest method for this problem is the enriched FVM, because it uses the piece-wise constant approximation in each cell, and no remeshing is needed.

Table 2.1: The computational time required to solve the discontinous SWE problem with 4 different methods. The enriched FVM is computationally the fastest method to solve this problem, closely followed by the conforming FVM and DG is a factor 3 slower than the FV methods.

Method	**CPU Time (s)**
Conforming FVM	23.145
Enriched FVM	18.669
Conforming DG	68.124
Enriched DG	57.938

2.8.4. The nonlinear 3D shallow water equations

The theory that was found about the enriched finite volume method is now applied to the full non-linear set of SWE to see if the method works in multiple dimensions. This full set of equations was given in Equation 2.53. This looks like a 2D set of equations, but the third dimension is given by the water height η. This set of equations is discretized using FVM with a multi-dimensional central difference approximation. With the following boundary conditions, and initial condition:

$$u(x = 0, y, t) = u(x = L_x, y, t) = v(x, y = 0, t) = v(x, y = L_y, t) = 0, \tag{2.68}$$

$$u(x, y, t_0) = v(x, y, t_0) = 0, \tag{2.69}$$

$$\eta(x, y, t_0) = A \cdot \cos\left(\frac{2\pi}{L_x}x\right) \cdot \cos\left(\frac{2\pi}{L_y}y\right). \tag{2.70}$$

The simulation is run to test the implementation of the full set of SWE. Snapshots of the simulation are given in Figure 2.17, for SWE with a sinewave as initial condition. The wave is oscillating due to the gravity and Buoyancy force.

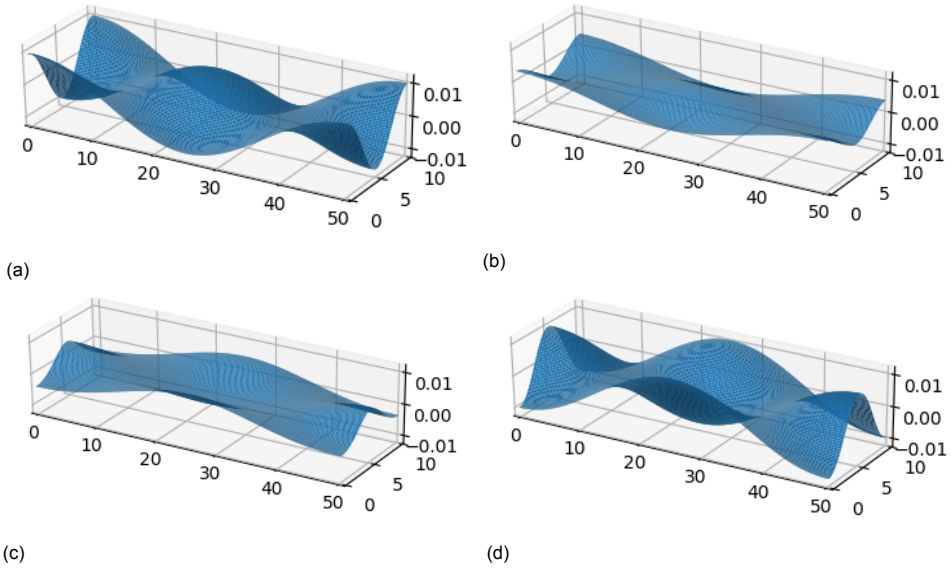

Figure 2.17: The simulation of the SWE with a sinewave as initial condition. The wave is oscillating due to gravity. A snapshot is taken at (a) 0.1s, (b) 0.6s, (c) 1.0s, and (d) 1.5s.

The next step is to add the wave-generator in the domain. This is done by changing the boundary conditions to

$$u(x = L_x, y, t) = v(x, y = 0, t) = v(x, y = L_y, t) = 0, \tag{2.71}$$

$$u(x, y, t_0) = v(x, y, t_0) = \eta(x, y, t_0) = 0, \tag{2.72}$$

$$u(x = 0, y, t) = A \cdot \sin(\omega t). \tag{2.73}$$

A simulation is made of a box filled with water with a wave generator on the left side of the domain. Snapshots of the simulation are given in Figure 2.18. The results are similar to the linearized set of equations in Equation 2.54.

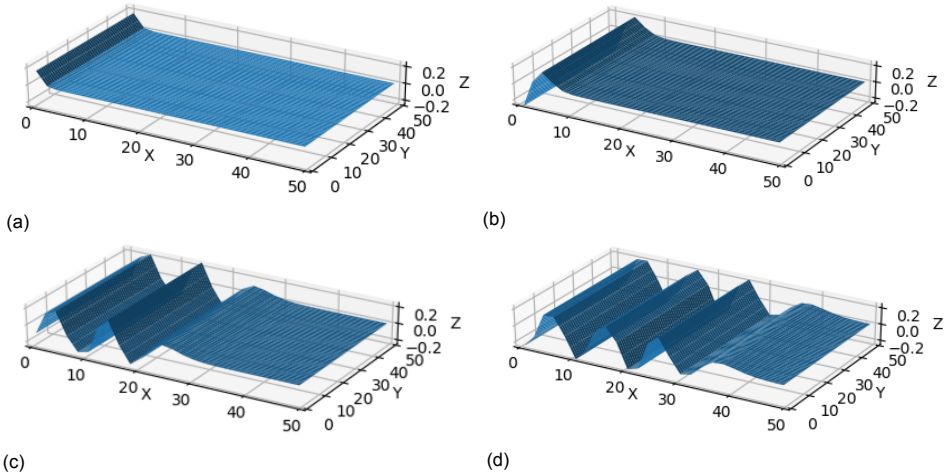

Figure 2.18: A box with a wave generator on one side of the domain. The sinusoidal motion of the wave generator gives the wave pattern. A snapshot is taken at (a) 1.0s, (b) 5.0s, (c) 20s, and (d) 30s.

2.9. Conclusions

This thesis has been concerned with the development of an enriched finite volume method. In order to get to this new method, different steps were taken. The first one was to get an overview of the existing methods. The methods that were explored were the finite volume method, the discontinuous Galerkin method and the enriched finite element method. Learning how these numerical methods discretize equations is necessary to find their differences and to see how elements of each method can be used in other methods. In order to do this, a relatively simple differential equation was taken: the linear advection equation. After discretizing this equation with the different methods, it was shown that the concepts of enriched FEM can be implemented in the finite volume method using discontinuous Galerkin. This is an important conclusion of this research. But many more conclusions can be drawn from this work. The first conclusion from the comparison of the methods is that the finite volume method is piece-wise constant DG method. This was a starting point for the development of the high-order FVM, and the enriched FVM. DG is a high-order extension of FVM, which is using a Galerkin least squares projection instead of the stencil approach from FVM. But this comes with higher computational costs, that's why in most fluid solvers use the FVM with its constant cell approximations. With the use of DG, the FVM solver can be kept untouched, and enrichments like high-order polynomials or discontinuous enrichment functions can be added.

2.9.1. A high-order finite volume method

In FEM high-order shape functions are introduced using the Legendre shape functions; this is called pFEM. The legendre shape functions are a set of orthogonal polynomials that is often used in pFEM. The same set of Legendre polynomials is also implemented in DG to get a high-order DG. This gives a better approximation of the solution of differential equations. In many problems local remeshing is needed to have a better approximation at locations where more accuracy is needed. This is for example due to a steep gradient of the solution in that part of the domain. The solution to this problem is usually remeshing. One option for this is to have a finer grid for the whole domain, but this takes more memory as more cell data has to be stored. The other solution is locally remeshing, so only around the more problematic or ”error-prone” area, the mesh is refined. The result is a non-uniform grid, and this grid needs to be regenerated when the discontinuity is moving over time. The high-order FVM proposed in this report adds locally a high-order polynomial approximation function. This high-order polynomial can be added on top of the standard, uniform FVM. The result is an accurate representation of the solution to a differential equation at location in the domain where that is needed. The addition of these high-order approximations in the FVM is an enrichment, because information about the solution of the problem is added in the formulation to locally improve the solution.

2.9.2. An enriched finite volume method

Enriched FEM decouples discontinuities like fluid-structure interfaces from the mesh. Using DG, the enrichments from FEM can be added to FVM. The result is a new non-conforming FVM: the enriched finite volume method. The main difference between this method and existing non-conforming FVMs is that this method decouples the discontinuities from the grid. The cut-cell method is also a non-conforming FVM, but this method uses an uniform grid and discontinuities like solids, or holes are added to the formulation by cutting existing cells. The immersed boundary method, which is also a non-conforming FVM, models discontinuities by using fibers. Therefore the structural response of this method is not accurate for solids immersed in the fluid. An enriched DG method is already developed, but DG takes approximately 3 times the CPU time of FVM. The enriched FVM combines both the computational speed of FVM, and the ability to resolve discontinuities accurately from enriched DG. The method recovers an optimal spatial convergence rate for a non-conforming discretization in FVM. In this report the enriched FEM that is considered is DE-FEM for strong discontinuities, but also other enriched formulations can be used. Examples of this are DE-FEM for both weak and strong discontinuities, or the enrichment function proposed by Möes with Heaviside step functions [67].

2.9.3. Recommendations for further work

This report introduces the new enriched finite volume method applied to the shallow water equations. But many more discontinuous problems can be solved using the enriched FVM. Examples of those are fluid-air interfaces, interaction of fluids with different densities, and also many more fluid-structure

interaction problems. An interesting further study could be on deformable structures immersed in fluid flow, where the fluids are solved with FVM and the structures with FEM. Different types of enrichment functions can be used in the method to solve different problems. The last recommendation is to test the method on benchmark problems to compare the method on its accuracy and required computational power. A standard benchmark problem used for FVM and DG is the stokes problem, which is one of the simplest unsteady problems derived from the Navier-Stokes equations that has an exact solution [68, 69].

3

Reflection

This chapter is a reflection on the process that led to an enriched finite volume method. The reflection is divided into 5 parts. The start of the thesis and literature review, the development of an enriched finite volume method, the results of this work, the planning, and some personal points of improvement.

3.1. The start of the project and literature study

After following the courses on Numerical Methods, Advanced FEM and its follow-up course Enriched FEM I developed a strong interest in the field of numerical methods. So a natural choice was to search for a thesis project in the field of FEM with Alejandro Aragon as supervisor. The first contact was made by e-mail and a meeting was organized in his office. We discussed the possibilities and the first plan was to continue the project on an enriched Stokes-Flow solver. But another possibility that Alejandro came up with was a collaboration project with Peter Wellens from Maritime Engineering. Alejandro his expertise is enriched FEM and Peters expertise is the finite volume method. Both methods are mathematical procedures to solve differential equations numerically. And both methods have their advantages and disadvantages and by comparing the two methods probably a new method could be developed which uses the beneficial properties of both methods. This sounded like a very interesting challenge, so I decided to take this project.

The first step was a meeting with both supervisors in which they explained their expectations of the project and shared some papers which served as a start of the literature research. The literature research was quite difficult as I only had basic knowledge of numerical methods from the master courses that I took on these subjects. Also there is much literature available on these methods in which even more cited papers are cited. So at a certain point I lost track of what to read and what to search for in literature. I contacted my supervisors and a meeting was set up in which a clearer direction of literature was pointed out. This helped me finish my literature study, which was a broad study on all numerical methods available ranging from the Finite Difference Method, Finite Volume Method and (Enriched) Finite Element Methods to more advanced derivatives of those methods like Discontinuos Galerkin FEM and Immersed FVM. The literature study was finished by presenting the literature to the Structural Optimization and Mechanics (SOM) research group. This presentation was held at the start of the summer holiday in July. The literature study was rewarded by the grade 8.0, which served as a good motivation to continue with my project.

3.2. The development of an enriched finite volume method

The project started where the literature study ended, namely with a comparison of the numerical methods available for a simple advection-diffusion problem. The aim of this comparison was to see how the different methods discretize the same methods on a simple 4 cell grid. The results of this sparked a great interest for the discontinuous Galerkin method, which was a method that I never used before that point, but seemed a very promising and active field of research. But at that point for me it was not clear in which way I could add something new to that method as it was already a hard task to fully grasp the method. I shared my concern with Peter that I was having difficulties in finding a gap in the knowledge which I could fill. Peter helped me very much on this point by giving me a set of equations

which are called the Shallow Water Equations (SWE). This is a set of equation with practical relevance and solves the Navier-Stokes equations for shallow water. A new approach was taken from that point which was a step-by-step approach to get to results to finish my thesis. Peter provided me with a FVM code which solves the SWE and my first task was to solve the same problem with a FEM method. This provided good insight in how both methods can be used to solve a system of equations. The next step was to solve the same set of equations, but now with a discontinuity. This aim of solving this discontinuous problem was to be able to use the concepts of enriched FEM, which is a computationally cheap method to discretize problems with discontinuities. First an enriched discontinuous Galerkin method was set up to solve this discontinuous problem and this led to the insight that FVM is actually a special case of DG. Knowing this the FVM can be raised to a higher order in a straightforward manner using Legendre polynomials and a high-order FVM was made. But more importantly the concept of enriched FEM could be brought into the FVM, which led to the development of the enriched FVM.

3.3. The results and the end of the project

After working 12 months on the project. The work and report were finished in April and the reviewing process started. My report was first review by Peter, who gave feedback on the work to improve the report. And this improved report was reviewed by Alejandro. At this point I found out that my academic writing skills were far below expected level, so a lot of improvement was needed to finish the thesis. After deleting a lot of unnecessary sections, and bringing the academic writing to an acceptable level green light was given at the start of July. The result of the thesis is a new enriched finite volume method, which can be used for fluid-structure interaction problems. The method is proved to be more efficient than conforming FVM and DG. Overal it was an educational process in which I improved my research skills, reading, writing and programming skills a lot. And the result is an interesting new method, which can be used for further research.

3.4. Planning and timeline

The literature presentation ended by giving the planning in a Gantt chart. A summary of the steps which I wanted to take to do the research is the following:

1. Solve a 1D advection-diffusion equation with the Finite Volume Method, FEM Method, Discontinuous Galerkin Method.
2. Solve the flexible wall in flow problem with the 3 methods.
3. See which fluid solver is most suited for enrichment functions.
4. Implement the enrichment functions in the fluid solver.
5. Solve some benchmark problems.

The first step was quickly finished as a big part of this step was already made during the literature study. But after that the original schedule which was supposed to be from July until the start of February was no longer followed. It took a long time to fully grasp all the methods that are available on such deep level, that is actually possible to extend and combine those methods. The flexible wall in flow problem was replaced by the shallow water equations in which waves were generated using a waveboard. When this was all finished in February the last three steps were followed. The enrichment functions were first implemented in DG and afterwards the methods were compared. And the end result are a very easy to implement high-order FVM and and enriched FVM.

3.5. Personal points of improvement

After a long project it is good to reflect on the work and see on which points I can improve in upcoming project work. At two points in this project I was really stuck and this could have been prevented. Engineering is all about project work, so it is important to write down the mistakes that I made during this project as points of improvement for upcoming projects in industry. My two main points of improvement are communication with the supervisors, time management and academic writing:

- Communication with the supervisors can be improved in 2 ways. The first one is to involve the supervisors more actively in my work. Especially in the first half of the project I only contacted the supervisors with my problems when it was already too late. I send them a message when I was really stuck in the project. So it was more or less an emergency call. What would have been way better and went much better in the second half of the project is to have regular meeting in which guidance of the supervisors is given. At the end of the project I was really stressed about the timeline, which led to me not being reasonable in my communication to my supervisors. I must improve at this point, because this behaviour is not tolerated.
- The second point of improvement is the planning. My original planning was not followed almost immediately since the start. According to my original planning my thesis would be finished at the start of February, but in practise it is finished end of June. Although it is hard to have a strict planning in research a time delay of 4 months is too much.
- The last point of improvement is academic writing. After a revision of my final report by Alejandro it became evident that my writing skills are far below academic level. Therefore, I was not ready to graduate. A lot of improvement in the writing style was needed to get the report to an acceptable level. Academic writing is a point where I still need to improve. The academic writing class given by my supervisor is very helpful for this.

Bibliography

[1] Jaime Peraire et al. “Adaptive remeshing for compressible flow computations”. In: *Journal of computational physics* 72.2 (1987), pp. 449–466.

[2] Darren DeZeeuw and Kenneth G Powell. “An adaptively refined Cartesian mesh solver for the Euler equations”. In: *Journal of Computational Physics* 104.1 (1993), pp. 56–68.

[3] Rainald Löhner. “A parallel advancing front grid generation scheme”. In: *International Journal for Numerical Methods in Engineering* 51.6 (2001), pp. 663–678.

[4] Bruce Wedan and J SOUTH JR. “A method for solving the transonic full-potential equation for general configurations”. In: *6th Computational Fluid Dynamics Conference Danvers*. 1983, p. 1889.

[5] G Yang et al. “A Cartesian cut cell method for compressible flows part A: Static body problems”. In: *The Aeronautical Journal* 101.1002 (1997), pp. 47–56.

[6] G Yang et al. “A cartesian cut cell method for compressible flows Part B: moving body problems”. In: *The Aeronautical Journal* 101.1002 (1997), pp. 57–65.

[7] David M Ingram, Derek M Causon, and Clive G Mingham. “Developments in Cartesian cut cell methods”. In: *Mathematics and Computers in Simulation* 61.3-6 (2003), pp. 561–572.

[8] Marsha Berger and Randall Leveque. “An adaptive Cartesian mesh algorithm for the Euler equations in arbitrary geometries”. In: *9th Computational Fluid Dynamics Conference*. 1989, p. 1930.

[9] James J Quirk. “An alternative to unstructured grids for computing gas dynamic flows around arbitrarily complex two-dimensional bodies”. In: *Computers & fluids* 23.1 (1994), pp. 125–142.

[10] G Yang, DM Causon, and DM Ingram. “Calculation of compressible flows about complex moving geometries using a three-dimensional Cartesian cut cell method”. In: *International Journal for Numerical Methods in Fluids* 33.8 (2000), pp. 1121–1151.

[11] S Cieslak et al. “Cut cell strategy for 3-D blast waves numerical simulations”. In: *Shock Waves* 10.6 (2001), pp. 421–429.

[12] Paul G Tucker and Zhiqiu Pan. “A Cartesian cut cell method for incompressible viscous flow”. In: *Applied Mathematical Modelling* 24.8-9 (2000), pp. 591–606.

[13] Tao Ye et al. “An accurate Cartesian grid method for viscous incompressible flows with complex immersed boundaries”. In: *Journal of computational physics* 156.2 (1999), pp. 209–240.

[14] Randall J LeVeque and Keh-Ming Shyue. “Two-dimensional front tracking based on high resolution wave propagation methods”. In: *Journal of Computational Physics* 123.2 (1996), pp. 354–368.

[15] Holavanahalli S Udaykumar et al. “Multiphase dynamics in arbitrary geometries on fixed Cartesian grids”. In: *Journal of Computational Physics* 137.2 (1997), pp. 366–405.

[16] Charles S Peskin. “Numerical analysis of blood flow in the heart”. In: *Journal of computational physics* 25.3 (1977), pp. 220–252.

[17] Richard P Beyer and Randall J LeVeque. “Analysis of a one-dimensional model for the immersed boundary method”. In: *SIAM Journal on Numerical Analysis* 29.2 (1992), pp. 332–364.

[18] Robert Dillon, Lisa Fauci, and Donald Gaver III. “A microscale model of bacterial swimming, chemotaxis and substrate transport”. In: *Journal of theoretical biology* 177.4 (1995), pp. 325–340.

[19] EA Fadlun et al. “Combined immersed-boundary finite-difference methods for three-dimensional complex flow simulations”. In: *Journal of computational physics* 161.1 (2000), pp. 35–60.

[20] Boyce E Griffith and Charles S Peskin. “On the order of accuracy of the immersed boundary method: Higher order convergence rates for sufficiently smooth problems”. In: *Journal of Computational Physics* 208.1 (2005), pp. 75–105.

[21] Wei-Xi Huang and Hyung Jin Sung. “An immersed boundary method for fluid–flexible structure interaction”. In: *Computer methods in applied mechanics and engineering* 198.33-36 (2009), pp. 2650–2661.

[22] Dokyun Kim and Haecheon Choi. “Immersed boundary method for flow around an arbitrarily moving body”. In: *Journal of Computational Physics* 212.2 (2006), pp. 662–680.

[23] Jungwoo Kim, Dongjoo Kim, and Haecheon Choi. “An immersed-boundary finite-volume method for simulations of flow in complex geometries”. In: *Journal of computational physics* 171.1 (2001), pp. 132–150.

[24] Yongsam Kim and Charles S Peskin. “Penalty immersed boundary method for an elastic boundary with mass”. In: *Physics of Fluids* 19.5 (2007), p. 053103.

[25] DV Le, BC Khoo, and KM Lim. “An implicit-forcing immersed boundary method for simulating viscous flows in irregular domains”. In: *Computer methods in applied mechanics and engineering* 197.25-28 (2008), pp. 2119–2130.

[26] John M Stockie and Sheldon I Green. “Simulating the motion of flexible pulp fibres using the immersed boundary method”. In: *Journal of Computational Physics* 147.1 (1998), pp. 147–165.

[27] Jin Wang and Anita Layton. “Numerical simulations of fiber sedimentation in Navier-Stokes flows”. In: *Communications in Computational Physics* 5.1 (2009), p. 61.

[28] Wing Kam Liu et al. “Immersed finite element method and its applications to biological systems”. In: *Computer methods in applied mechanics and engineering* 195.13-16 (2006), pp. 1722–1749.

[29] Lucy Zhang et al. “Immersed finite element method”. In: *Computer Methods in Applied Mechanics and Engineering* 193.21-22 (2004), pp. 2051–2067.

[30] Lucy T Zhang and Mickaël Gay. “Immersed finite element method for fluid-structure interactions”. In: *Journal of Fluids and Structures* 23.6 (2007), pp. 839–857.

[31] Yuri Bazilevs, Kenji Takizawa, and Tayfun E Tezduyar. *Computational fluid-structure interaction: methods and applications*. John Wiley & Sons, 2013.

[32] Douglas N Arnold et al. “Unified analysis of discontinuous Galerkin methods for elliptic problems”. In: *SIAM journal on numerical analysis* 39.5 (2002), pp. 1749–1779.

[33] Francesco Bassi and Stefano Rebay. “A high-order accurate discontinuous finite element method for the numerical solution of the compressible Navier–Stokes equations”. In: *Journal of computational physics* 131.2 (1997), pp. 267–279.

[34] Bernardo Cockburn, George E Karniadakis, and Chi-Wang Shu. *Discontinuous Galerkin methods: theory, computation and applications*. Vol. 11. Springer Science & Business Media, 2012.

[35] Carlos Erik Baumann and J Tinsley Oden. “A discontinuous hp finite element method for convection—diffusion problems”. In: *Computer Methods in Applied Mechanics and Engineering* 175.3-4 (1999), pp. 311–341.

[36] Paul Castillo et al. “An a priori error analysis of the local discontinuous Galerkin method for elliptic problems”. In: *SIAM Journal on Numerical Analysis* 38.5 (2000), pp. 1676–1706.

[37] Bernardo Cockburn and Chi-Wang Shu. “The local discontinuous Galerkin method for time-dependent convection-diffusion systems”. In: *SIAM Journal on Numerical Analysis* 35.6 (1998), pp. 2440–2463.

[38] Kun Wang, Linbo Zhang, and Zhangxin Chen. “Development of discontinuous galerkin methods and a parallel simulator for reservoir simulation”. In: *SPE/IATMI Asia Pacific Oil & Gas Conference and Exhibition*. OnePetro. 2015.

[39] Bernardo Cockburn et al. “Local discontinuous Galerkin methods for the Stokes system”. In: *SIAM Journal on Numerical Analysis* 40.1 (2002), pp. 319–343.

[40] Béatrice Rivière, Mary F Wheeler, and Vivette Girault. “Improved energy estimates for interior penalty, constrained and discontinuous Galerkin methods for elliptic problems. Part I”. In: *Computational Geosciences* 3.3 (1999), pp. 337–360.

[41] Yulong Xing. “Exactly well-balanced discontinuous Galerkin methods for the shallow water equations with moving water equilibrium”. In: *Journal of Computational Physics* 257 (2014), pp. 536–553.

[42] Francis X Giraldo, Jan S Hesthaven, and Tim Warburton. “Nodal high-order discontinuous Galerkin methods for the spherical shallow water equations”. In: *Journal of Computational Physics* 181.2 (2002), pp. 499–525.

[43] Niklas Wintermeyer et al. “An entropy stable nodal discontinuous Galerkin method for the two dimensional shallow water equations on unstructured curvilinear meshes with discontinuous bathymetry”. In: *Journal of Computational Physics* 340 (2017), pp. 200–242.

[44] Khosro Shahbazi, Paul F Fischer, and C Ross Ethier. “A high-order discontinuous Galerkin method for the unsteady incompressible Navier–Stokes equations”. In: *Journal of computational physics* 222.1 (2007), pp. 391–407.

[45] Jian-Guo Liu and Chi-Wang Shu. “A high-order discontinuous Galerkin method for 2D incompressible flows”. In: *Journal of Computational Physics* 160.2 (2000), pp. 577–596.

[46] Lucas C Wilcox et al. “A high-order discontinuous Galerkin method for wave propagation through coupled elastic–acoustic media”. In: *Journal of Computational Physics* 229.24 (2010), pp. 9373–9396.

[47] Xiu Ye. “A new discontinuous finite volume method for elliptic problems”. In: *SIAM Journal on Numerical Analysis* 42.3 (2004), pp. 1062–1072.

[48] Xiu Ye. “A discontinuous finite volume method for the Stokes problems”. In: *SIAM Journal on Numerical Analysis* 44.1 (2006), pp. 183–198.

[49] Gang Wang, Yinnian He, and Rui Li. “Discontinuous finite volume methods for the stationary Stokes–Darcy problem”. In: *International Journal for Numerical Methods in Engineering* 107.5 (2016), pp. 395–418.

[50] BR Baliga and SV Patankar. “A new finite-element formulation for convection-diffusion problems”. In: *Numerical Heat Transfer* 3.4 (1980), pp. 393–409.

[51] Zhiqiang Cai. “On the finite volume element method”. In: *Numerische Mathematik* 58.1 (1990), pp. 713–735.

[52] Ivo Babuška, Gabriel Caloz, and John E Osborn. “Special finite element methods for a class of second order elliptic problems with rough coefficients”. In: *SIAM Journal on Numerical Analysis* 31.4 (1994), pp. 945–981.

[53] Jens M Melenk and Ivo Babuška. “The partition of unity finite element method: basic theory and applications”. In: *Computer methods in applied mechanics and engineering* 139.1-4 (1996), pp. 289–314.

[54] Nicolas Moës, John Dolbow, and Ted Belytschko. “A finite element method for crack growth without remeshing”. In: *International journal for numerical methods in engineering* 46.1 (1999), pp. 131–150.

[55] S Jamshidi and N Fallah. “Extended finite volume method with enriched HPCK shape functions for dynamic crack propagation modeling”. In: *Engineering Fracture Mechanics* 239 (2020), p. 107327.

[56] Davide Cortinovis and Patrick Jenny. “Iterative Galerkin-enriched multiscale finite-volume method”. In: *Journal of Computational Physics* 277 (2014), pp. 248–267.

[57] Bernardo Cockburn and Chi-Wang Shu. “The Runge–Kutta discontinuous Galerkin method for conservation laws V: multidimensional systems”. In: *Journal of Computational Physics* 141.2 (1998), pp. 199–224.

[58] Ludovic Noels and Raúl Radovitzky. “An explicit discontinuous Galerkin method for non-linear solid dynamics: Formulation, parallel implementation and scalability properties”. In: *International Journal for Numerical Methods in Engineering* 74.9 (2008), pp. 1393–1420.

[59] SeeChew Soon. *Hybridizable discontinuous Galerkin method for solid mechanics*. University of Minnesota, 2008.

[60] W H Reed and T R Hill. “Triangular mesh methods for the neutron transport equation”. In: (Oct. 1973). URL: https://www.osti.gov/biblio/4491151.

[61] Bernardo Cockburn, George E. Karniadakis, and Chi-Wang Shu. “The Development of Discontinuous Galerkin Methods”. In: *Discontinuous Galerkin Methods*. Ed. by Bernardo Cockburn, George E. Karniadakis, and Chi-Wang Shu. Berlin, Heidelberg: Springer Berlin Heidelberg, 2000, pp. 3–50. ISBN: 978-3-642-59721-3.

[62] PC McCarthy, JE Sayre, and BLR Shawyer. “Generalized legendre polynomials”. In: *Journal of mathematical analysis and applications* 177.2 (1993), pp. 530–537.

[63] CA Duarte et al. “A generalized finite element method for the simulation of three-dimensional dynamic crack propagation”. In: *Computer methods in applied mechanics and engineering* 190.15-17 (2001), pp. 2227–2262.

[64] Alejandro M Aragón and Angelo Simone. “The discontinuity-enriched finite element method”. In: *International Journal for Numerical Methods in Engineering* 112.11 (2017), pp. 1589–1613.

[65] PL Butzer and R Weis. “On the Lax equivalence theorem equipped with orders”. In: *Journal of Approximation Theory* 19.3 (1977), pp. 239–252.

[66] John Crank and Phyllis Nicolson. “A practical method for numerical evaluation of solutions of partial differential equations of the heat-conduction type”. In: *Mathematical Proceedings of the Cambridge Philosophical Society*. Vol. 43. 1. Cambridge University Press. 1947, pp. 50–67.

[67] Nicolas Moës et al. “A computational approach to handle complex microstructure geometries”. In: *Computer methods in applied mechanics and engineering* 192.28-30 (2003), pp. 3163–3177.

[68] CY Wang. “Exact solutions of the steady-state Navier-Stokes equations”. In: *Annual Review of Fluid Mechanics* 23 (1991), pp. 159–177.

[69] GK Batchelor. “Fluid Mechanics. By LD LANDAU and EM LIFSHITZ. 2nd English edition. Pergamon Press, 1987.” In: *Journal of Fluid Mechanics* 205 (1989), pp. 593–594.